1.0

1.1

1.25

4.5
5.0
5.6

2.8
3.2
3.6
4.0

1.4

2.5
2.2
2.0
1.8
1.6

MICROCOPY RESOLUTION TEST CHART
NATIONAL BUREAU OF

AFWAL-TR-81-1163

ADA110290

PHASE EFFECTS OF IONOSPHERIC IRREGULARITIES

Results of the Air Force Wright Aeronautical Data Processing Effort

CLIFFORD W. PRETTIE

BERKELEY RESEARCH ASSOCIATES
P. O. BOX 983
BERKELEY, CALIFORNIA 94701

DTIC
S ELECTE D
FEB 1 1982
B

SEPTEMBER 1981

FINAL REPORT FOR PERIOD JANUARY 1979 — JULY 1981

AVIONICS LABORATORY
AIR FORCE WRIGHT AERONAUTICAL LABORATORIES
AIR FORCE SYSTEMS COMMAND
WRIGHT- PATTERSON AIR FORCE BASE, OHIO 45433

82 02 01 029

ALLEN L. JOHNSON
Project Engineer, AFWAL/AAAD

CHARLES C. GAUDER
Chief, Information Transmission Branch
Avionics Laboratory

FOR THE COMMANDER

RICHARD H. BOIVIN, COL, USAF
Chief, System Avionics Division
Avionics Laboratory

REPORT DOCUMENTATION PAGE		READ INSTRUCTIONS BEFORE COMPLETING FORM
1. REPORT NUMBER AFWAL-TR-81-1163	2. GOVT ACCESSION NO. AD-A110290	3. RECIPIENT'S CATALOG NUMBER
4. TITLE (and Subtitle) PHASE EFFECTS OF IONOSPHERIC IRREGULARITIES-- RESULTS OF THE AIR FORCE WRIGHT AERONAUTICAL DATA PROCESSING EFFORT		5. TYPE OF REPORT & PERIOD COVERED Final Report 1 Jan 79 - 31 Jul 81
		6. PERFORMING ORG. REPORT NUMBER PD-BRA-81-244R
7. AUTHOR(s) Clifford W. Prettie		8. CONTRACT OR GRANT NUMBER(s) DNA001-79-C-0141
9. PERFORMING ORGANIZATION NAME AND ADDRESS Berkeley Research Associates P.O. Box 983 Berkeley, CA 94701		10. PROGRAM ELEMENT, PROJECT, TASK AREA & WORK UNIT NUMBERS 1227/03/13
11. CONTROLLING OFFICE NAME AND ADDRESS Director Defense Nuclear Agency Washington, DC 20305		12. REPORT DATE September 1981
		13. NUMBER OF PAGES 93
14. MONITORING AGENCY NAME & ADDRESS(If different from Controlling Office) Avionics Laboratory (AFWAL/AAAD) Air Force Wright Aeronautical Laboratories Wright-Patterson AFB, OH 45433		15. SECURITY CLASS. (of this report) UNCLASSIFIED
		15a. DECLASSIFICATION/DOWNGRADING SCHEDULE

16. DISTRIBUTION STATEMENT (of this Report)

Approved for Public Release; Distribution Unlimited

17. DISTRIBUTION STATEMENT (of the abstract entered in Block 20, If different from Report)

18. SUPPLEMENTARY NOTES

19. KEY WORDS (Continue on reverse side if necessary and identify by block number)

satellite communications	barium release	phase noise
ionospheric effects	CASTOR	sine transform
amplitude scintillations	equatorial irregularities	power law fit
phase scintillations	polar irregularities	
ionospheric heating	aircraft dynamics	

20. ABSTRACT (Continue on reverse side if necessary and identify by block number)

Data processing of Air Force Wright Aeronautical Laboratory flight test
satellite signal measurements has been performed to illustrate the phase effects
associated with ionospheric irregularities. Measurements are available at 250 MHz
satellite signals traversing ionospheric heating induced irregularities, barium ion
cloud irregularities, and polar and equatorial irregularities. For each of these
environments displays of amplitude, phase phase difference standard deviation,
phase difference histograms and phase power spectral density are given.
The results of ionospheric heating measurements imply that underdense heating
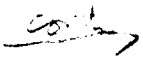
DD FORM 1473 EDITION OF 1 NOV 65 IS OBSOLETE

20.   ABSTRACT (Continued)

produces large scale irregularities with fluctuation levels that are conceivably larger than overdense heating fluctuations.

The barium measurements from the CASTOR releases by Max Planck Institute in March 1979 near Peru show no barium associated phase effects. Because of the 275 km release altitude it is expected that the associated phase effects should be difficult to resolve.

The phase difference histograms from the strong fading observed in the polar and equatorial measurements illustrate the importance of the non-Gaussian nature of the phase to communications. Binary phase-shift keyed (BPSK) irreducible error rates greater than 10^{-3} are predicted for these environments based upon their similarity with band-limited Gaussian noise.

PREFACE

    The author would like to express his gratitude
to Air Force Wright Aeronautical Laboratory/AAAD for
their close cooperation and for the opportunity to
reduce this highly interesting set of data.

    He would also like to acknowledge the dedicated
efforts of John Ferrante of Berkeley Research Associates
who performed much of the data processing behind the
results presented herein.

CONTENTS

ILLUSTRATIONS

4

5

TABLES

SECTION 1

INTRODUCTION

Ionospheric propagation data obtained by the AAAD division of Air Force Wright Aeronautical Laboratory (AFWAL) has been processed to illustrate the phase effects associated with scintillations. The data was obtained from flight test measurements of satellite signals propagating through naturally and artifically disturbed ionospheres. The effects of natural ionospheric disturbances were measured in both the equatorial and polar regions. Artificial disturbance measurements were made through the ionospheric environments produced by a high altitude equatorial barium release and by the Platteville ionospheric heater. The flight test measurements were performed during the period of January 1979 through April 1980. Data processing was performed over the period September 1980 through April 1981. The purpose of this report is to present the results of this data processing.

Section 2 presents a discussion of the propagation environments measured and illustrates the basic effects observed. Representative amplitude and phase plots are shown. The phase plots for the Platteville heater experiment flight tests are the first available from this type of ionospheric modification (to the author's knowledge).

Section 3 presents further analyses of the phase data. It discusses and gives examples of various phase descriptions such as the phase power spectral density and the variance of the phase difference over a specified interval. It also discusses the implications of phase effects to the performance of satellite communications.

8

Section 4 discusses the ionospheric structures inferrable from the data. Results of back propagation attempts are given. A brief discussion of aircraft dynamics phase effects is also given.

Section 5 presents conclusions about the nature of the phase effects observed and the propagation media producing them. Recommendations for future measurements and data processing are given.

SECTION 2

SATELLITE SIGNAL MEASUREMENTS

Measurements of four different types of disturbed ionospheric media were available for data processing in the form of eight different files. This section presents a qualitative description of the scintillation effects for each of these environments through amplitude and phase plots from each of the data files. A brief discussion of the measurements and software processing is also given.

The ionospheric media, satellite signal sources, and dates of measurement for each of the files is listed in Table 2-1. Also given is a one word description of the amplitude fading observed. As the UHF signal measurements were made without doppler correction, files in which little or no fading was observed are useful for establishing a phase stability reference and are labelled "quiet" in the table.

2-1   MEASUREMENT AND SOFTWARE PROCESSING SUMMARY.

Before presenting amplitude and phase plots it is appropriate to review the measurement and software processing techniques used to present the data.

Each of the four satellites used in the measurements broadcasted c.w. UHF signals at approximately 250 MHz. The signals from the SDS satellite were somewhat exceptional in that the satellite would change its transmit frequency approximately every 100 seconds. This change accommodates doppler track through SDS's eccentric polar orbit but

10

Table 2-1. Ionospheric measurements.

Item	Date month/day/year	Medium	Satellite	Fading Intensity
1	4/16/80	–	LES-8	quiet
2	5/13/80	Platteville over-dense heating	LES-9	moderate
3	4/16/80	Platteville under-dense heating	LES-8	weak
4	1/26/79	–	SDS	quiet
5	1/26/79	polar irregularities	SDS	strong
6	12/19/79	–	FLTSAT	quiet
7	12/19/79	equatorial irregularities	FLTSAT	strong
8	3/23/79	equatorial barium release	LES-9	weak

requires extra attention in the software processing to allow presentation of continuous phase.

The satellite signals were received by the AFWAL 662 aircraft. This aircraft is a modified KC-135 (similar to a Boeing 707) which travels at roughly 225 meters per second and which is heavily instrumented for satellite signal reception and diagnostics. The 662 aircraft provides an excellent platform from which to perform satellite signals measurements and has been used extensively in other important ionospheric measurement programs such as the DNA PLACES and STRESS programs and the AFGL equatorial campaign. While doppler correction of UHF signals is possible through the use of received K-band signals when operating with LES-8 or LES-9, for the measurements discussed herein none was employed. Thus the intrinsic dynamic stability of the aircraft in straight-and-level flight at altitudes above 30,000 feet is relied upon in place of K-band doppler correction.

The received UHF signals were down-converted by a fixed frequency local oscillator system to a signal with a frequency low enough to be suitable for analog recording, typically 500 Hz. The analog recordings from the various dates of Table 2-1 were digitized at 4,000 11-bit samples per second into numerous data files which were provided for the software processing effort.

To perform the software processing a tunable demodulator was implemented to perform calculations of the coherent and quadrature components of the down-converted signals. From these quantities the signal amplitude and phase have been calculated both for displays and for use in subsequent processing. Key to the processing was the

12

manner in which the demodulator was tuned. The tuning strategy chosen was to set the local oscillator frequency according to the parabolic time dependence determined from a fit to the dependence of the signal frequency observed in spectra taken throughout the data interval. This strategy is in accord with the fact that satellite doppler to an aircraft flying straight-and-level has ideally a dependence very close to parabolic. Moreover, this strategy produces reasonable results and does not introduce unpredictable artifact.

For display purposes the phase is further processed to enhance its high-pass features. High-pass filtering is implemented by differing the phase with the output of a 2-pole Butterworth low-pass filter with break point at .1 Hz. Thus, features with periods longer than 10 seconds are present in the high-pass phase display but with amplitudes reduced from the levels produced by the demodulator processing. Note that this filtering is performed only for phase data display.

2-2   PLATTEVILLE HEATER MEASUREMENTS

Measurements are available from the ionospheric disturbances created by the NOAA-operated Platteville heater during March and April 1980 (Johnson and Wright, 1980, Ref. 1). The heater is a high powered HF transmitter which is capable of producing field aligned ionospheric irregularities and has been well documented in the literature (Utlaut and Violette, 1974, Ref. 2, L.M. Duncan, 1981, Ref. 3). The irregularities have scale sizes typically .5 to 1 kilometer and produce a 2-10% modulation of electron density. Early observations of radio star scintillations

at 40 MHz caused by the irregularities were made by
Rufenach (1973, Ref. 4). Early satellite scintillation
measurements were made by Bowhill (1974, Ref. 5). These
early observations were made primarily for the case of over-
dense heating, i.e., HF transmission below the critical F-
layer frequency. The heater experiments performed in the
March-April 1980 time period, from which the measurements
discussed herein came, included underdense heating. Results
of amplitude observations from these experiments have been
reported in Basu, et al. (1980, Ref. 6 and 1981, Ref. 7).

Figures 2-1 and 2-2 illustrate the amplitude and
phase respectively for the reference file. One minute of
amplitude data is shown in Figure 2-1 which depicts the
fluctuations associated with the noise. Four minutes of
phase data are shown in Figure 2-2. The fluctuations
demonstrate the phase stability available. Possible sources
of the fluctuations include natural ionospheric total
electron content fluctuations of order 10^{15} electrons per
meter squared, aircraft dynamic displacements of order 1
meter, atmospheric column density changes of order 4 grams
per square centimeter, and satellite oscillator instability
of order 1 part in 10^{10} over 30 seconds. The feature at the
right-hand side of the plot is unusual in its appearance and
magnitude and may be associated with a one-time ionospheric
phenomenon or aircraft maneuver. No other such feature
occurs during the eight minutes of data available.

The scintillation for the case of overdense heating
is illustrated in Figures 2-3 and 2-4. Over the interval
0203-0207 the amplitude scintillations were observed to
build up to the level illustrated in the one minute plot
of Figure 2-3 for the period 0206-0207. Scintillations
produced fading as deep as 8 dB with an approximate rate of
1 fade every 2 seconds. The phase plot of Figure 2-4 shows

14
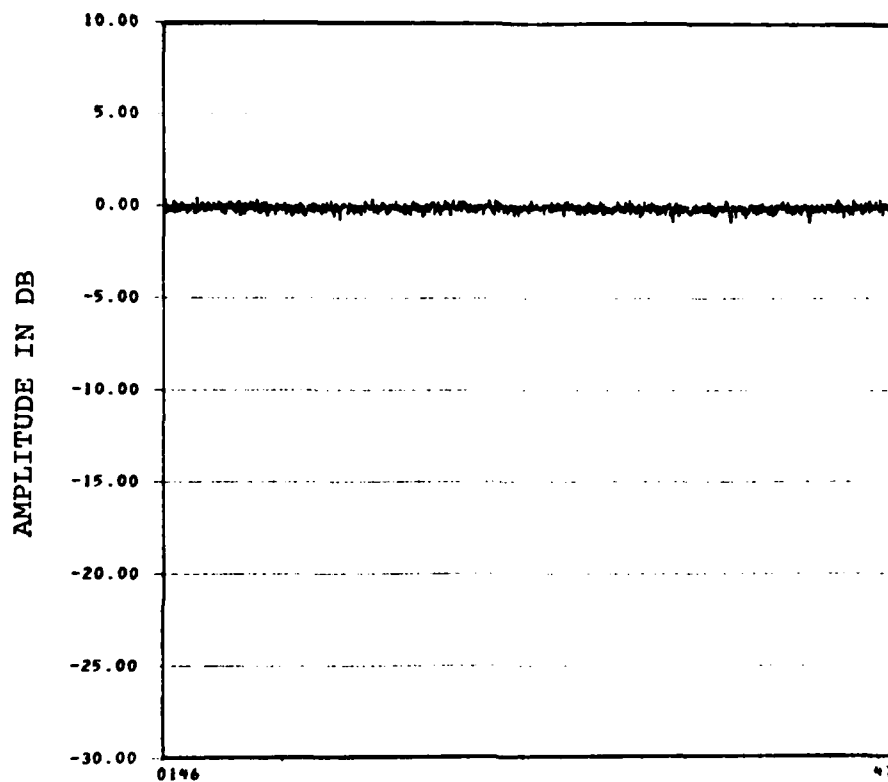
ZULU TIME

LES-8 FILE 1

Figure 2-1. Amplitude of LES-8 UHF signal
during quiet portion of the
16 April 1980 Platteville flight
test.

15
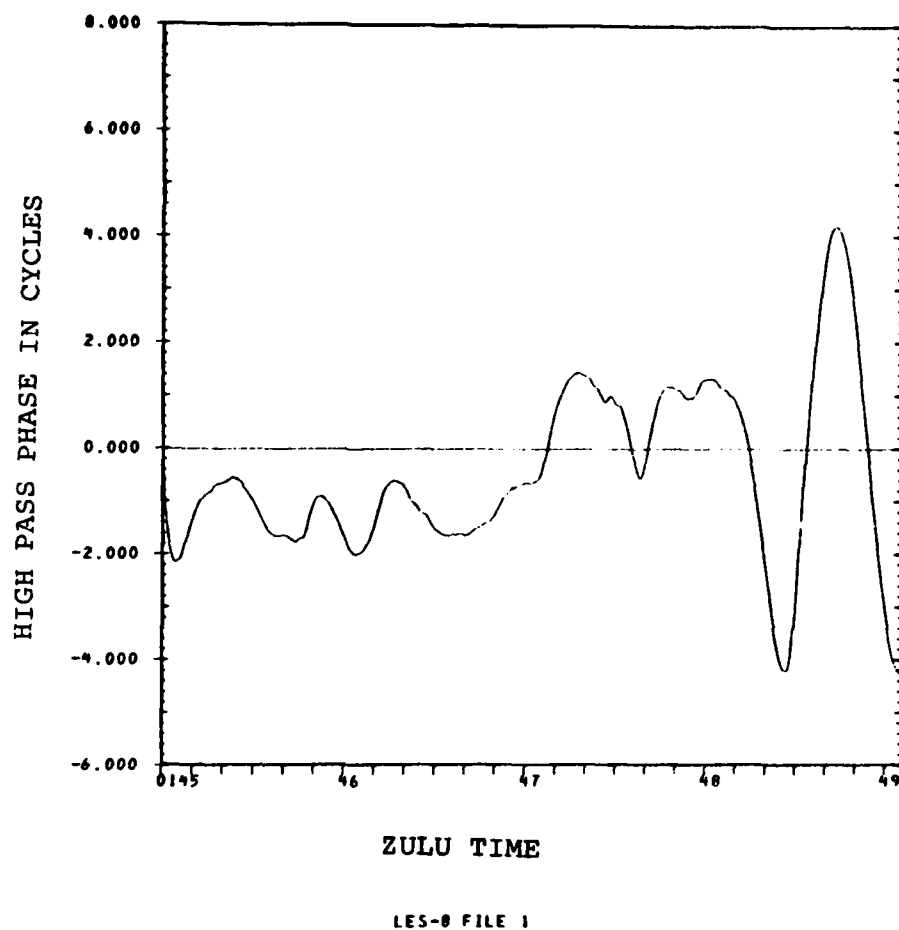
Figure 2-2.   Phase of LES-8 UHF signal during
quiet portion of the 16 April 1980
Platteville flight test.

16
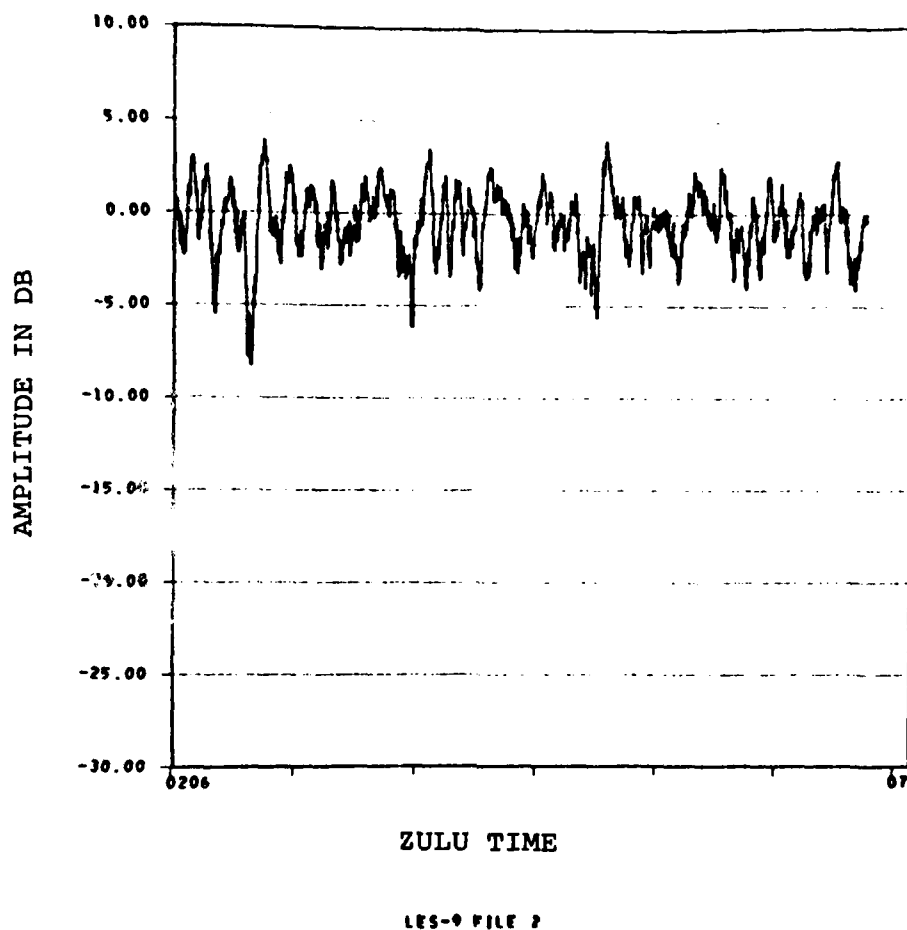
Figure 2-3. Amplitude of LES-9 fading UHF signal measured during the 13 March 1980 flight test near Platteville. The ionosphere was being heated in the overdense mode.

ZULU TIME
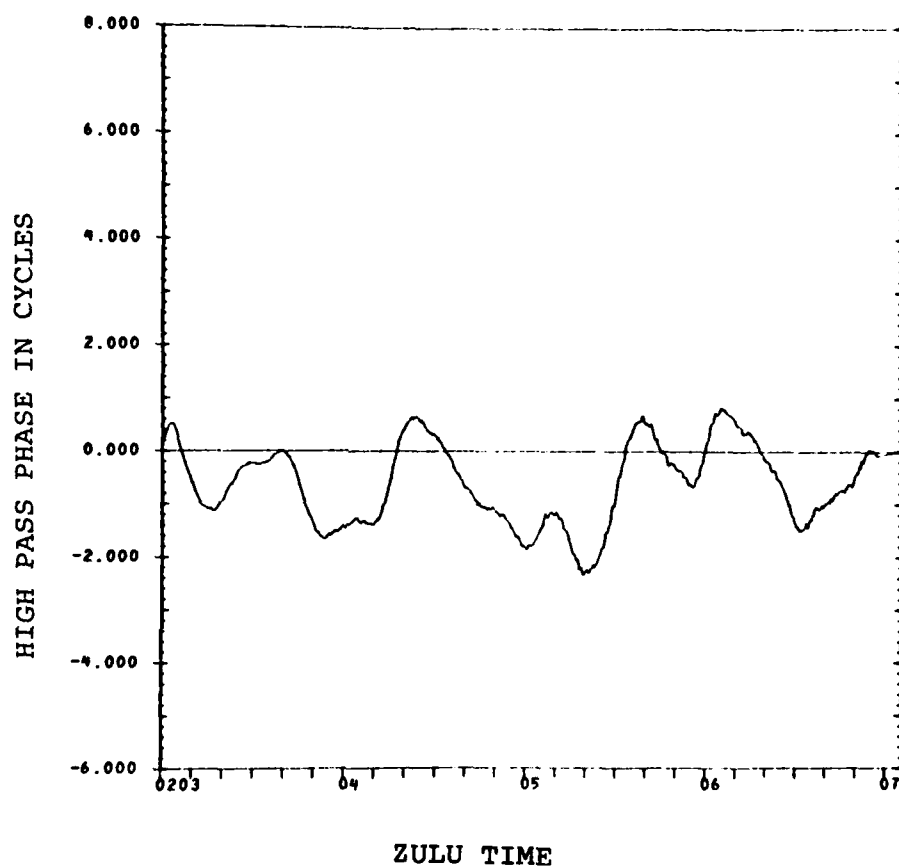
LES-9 FILE 2

Figure 2-4. Phase of LES-9 fading UHF signal measured during the 13 March 1980 flight test near Platteville. The ionosphere was being heated in the overdense mode.

18

phase fluctuations with the same magnitude or less (!) than
the fluctuations seen in the phase reference plot of
Figure 2-3. These gross fluctuations may even have arisen
from some souce other than overdense heating of the
ionosphere. Superimposed on these fluctuations, however,
are high frequency fluctuations with a steadily increasing
magnitude. These fluctuations represent scintillation
phase effects.

Figures 2-5 and 2-6 illustrate the situation observed
when the heater is operated in the underdense mode. Figure
2-5 illustrates the amplitude fading over one minute of
data. Strip chart data published in Ref. 1 showing the
amplitude variations over this same time period indicate
small amplitude fluctuations of order 1 dB. These fluctua-
tions are not as easily seen in the plot of Figure 2-5.
Higher resultion plots with various signal and video filtering
bandwidths reveal several features which match those displayed
in Reference 1. From this processing two conclusions were
derived. First, the digital signal is noisier than the
original signal (by at least 6 dB) and second, the strip
chart calibration (shown in Ref. 1) exaggerates the dB
fluctuations by an approximate factor of 2. The phase
fluctuations of Figure 2-6 are surprising in their magnitude.
These fluctuations are significantly larger than those seen
in the phase stability reference of Figures 2-2 and can be
attributed to the effects of underdense heating.

2-3   POLAR MEASUREMENTS

Measurements of scintillations of SDS satellite signals
from a flight above the auroral oval on 26 January 1979 were

19

Figure 2-5. Amplitude of LES-8 UHF signal measured during the 16 April 1980 flight test of the effects of underdense ionospheric heating at Platteville.

20

HIGH PASS PHASE IN CYCLES
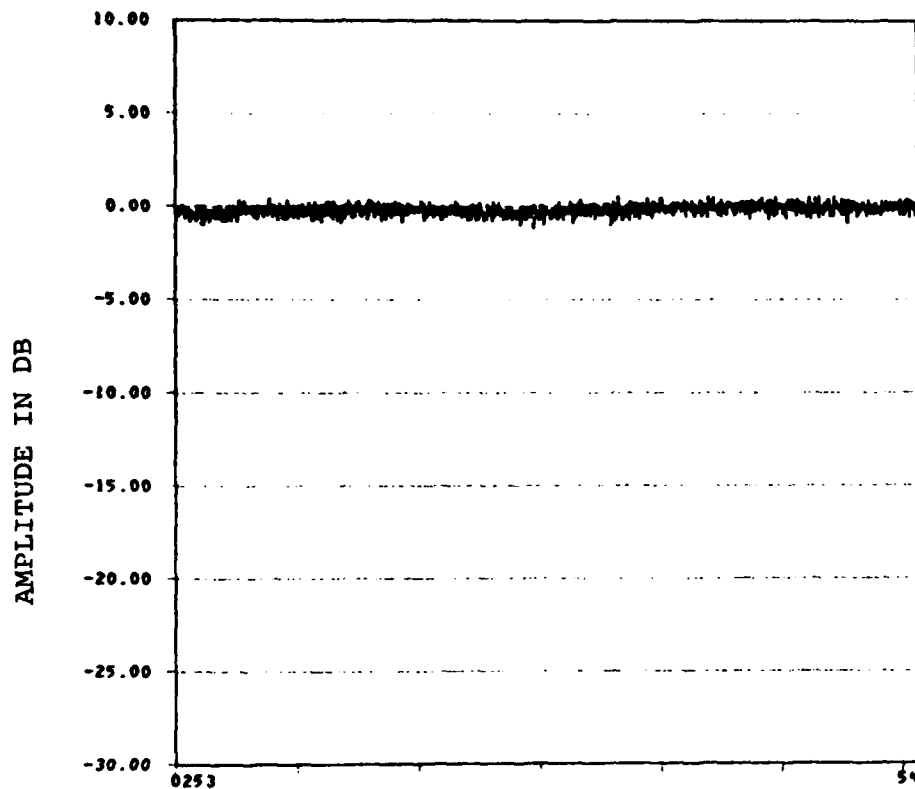
ZULU TIME
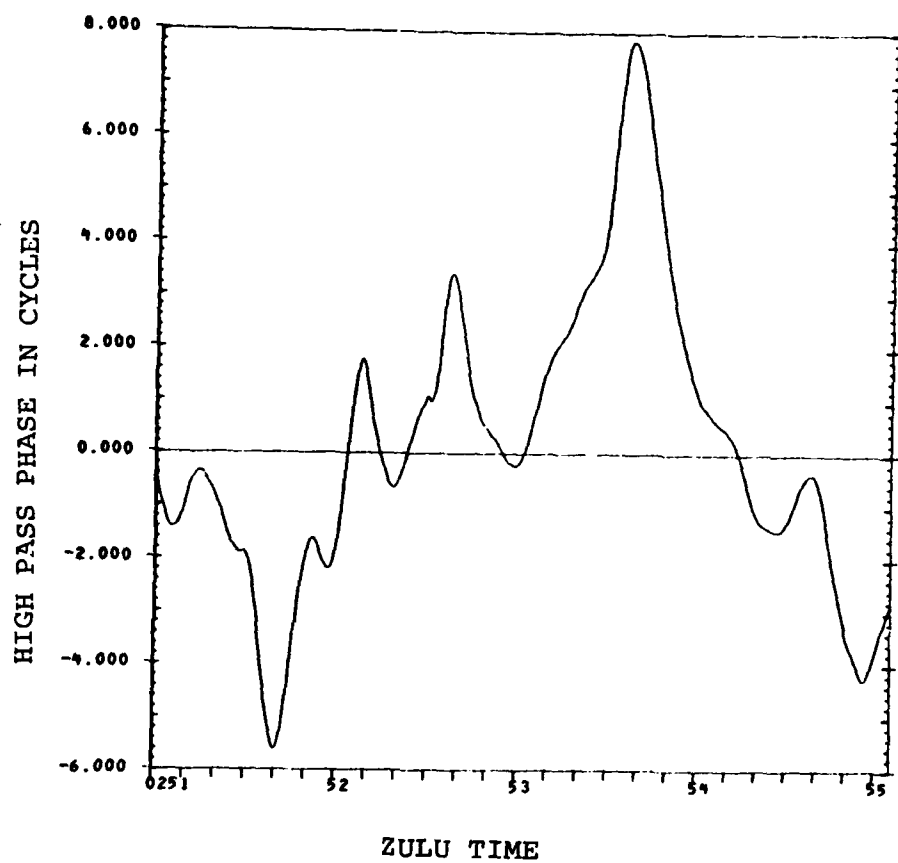
LES-8 FILE 2

Figure 2-6.   Phase of LES-8 UHF signal measured
during the 16 April 1980 flight test
of the effects of underdense ionospheric
heating at Platteville.

21

available for processing. During the majority of this flight scintillations were observed. Figures 2-7 and 2-8 show the amplitude and phase from a portion of the flight in which the scintillations were weak. The fading shown in the one minute plot of Figure 2-7 is 3 dB or less. The phase plot of Figure 2-8, thus, represents a phase stability reference for a signal through weak ionospheric irregularities. Note that the fluctuation magnitude is comparable to that observed from LES-8 during Platteville measurements shown in Figure 2-2.

Figures 2-9 and 2-10 illustrate the signal structure during strong fading. The four minute time interval displayed presents some of the fastest fading observed during the flight. Figure 2-9 illustrates one minute of amplitude fading. Focuses as strong as 5 dB and fades as deep as 30 dB can be seen. The phase shown in Figure 2-10 displays the typical characteristics of a strongly fading environment. Numerous phase slope discontinuities are apparent in the data.

Both amplitude and phase measurements of polar scintillations have been performed in the past (examples include Fremouw, et al., 1978, Ref. 8, Basu and Aarons, 1980, Ref. 9 and Rino and Matthews, 1980, Ref. 10). Phase measurements have been made primarily with the use of the WIDEBAND satellite. The phase measurements of Figure 2-10 are (to the author's knowledge) the first to be made using a relatively stationary satellite.

2-4   EQUATORIAL MEASUREMENTS

As in the case of the natural polar environment, numerous measurements of amplitude and phase scintillations

ZULU TIME

POLAR REEL 2
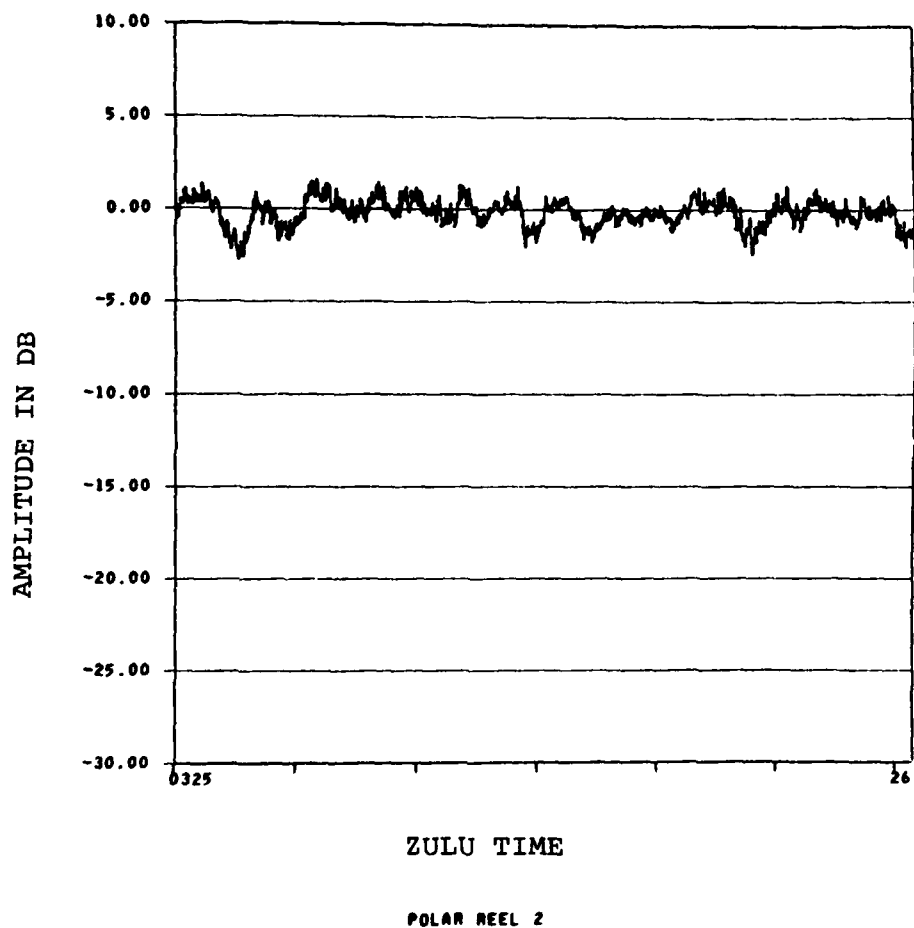
Figure 2-7. Amplitude of SDS UHF signal measured
during some of weakest fading observed
on the 26 January 1979 polar flight
test above the auroral oval.

23
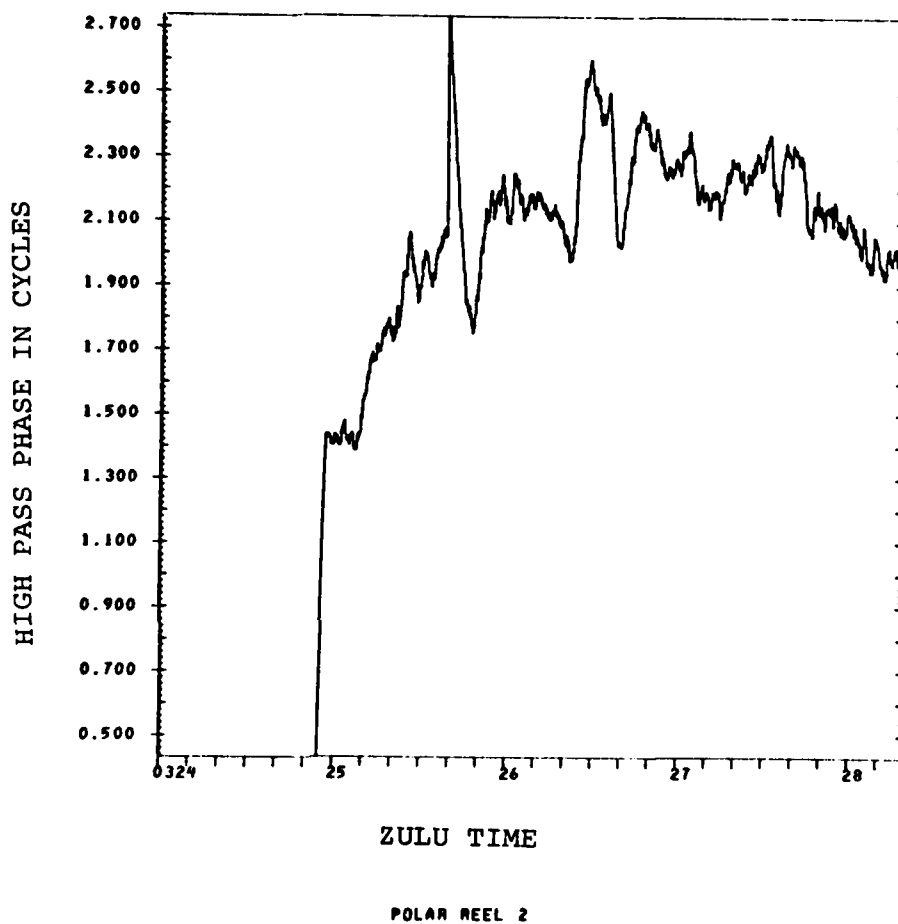
Figure 2-8.   Phase of SDS UHF signal measured during some of weakest fading observed on the 26 January 1979 polar flight test above the auroral oval.

24

ZULU TIME

POLAR REEL 4
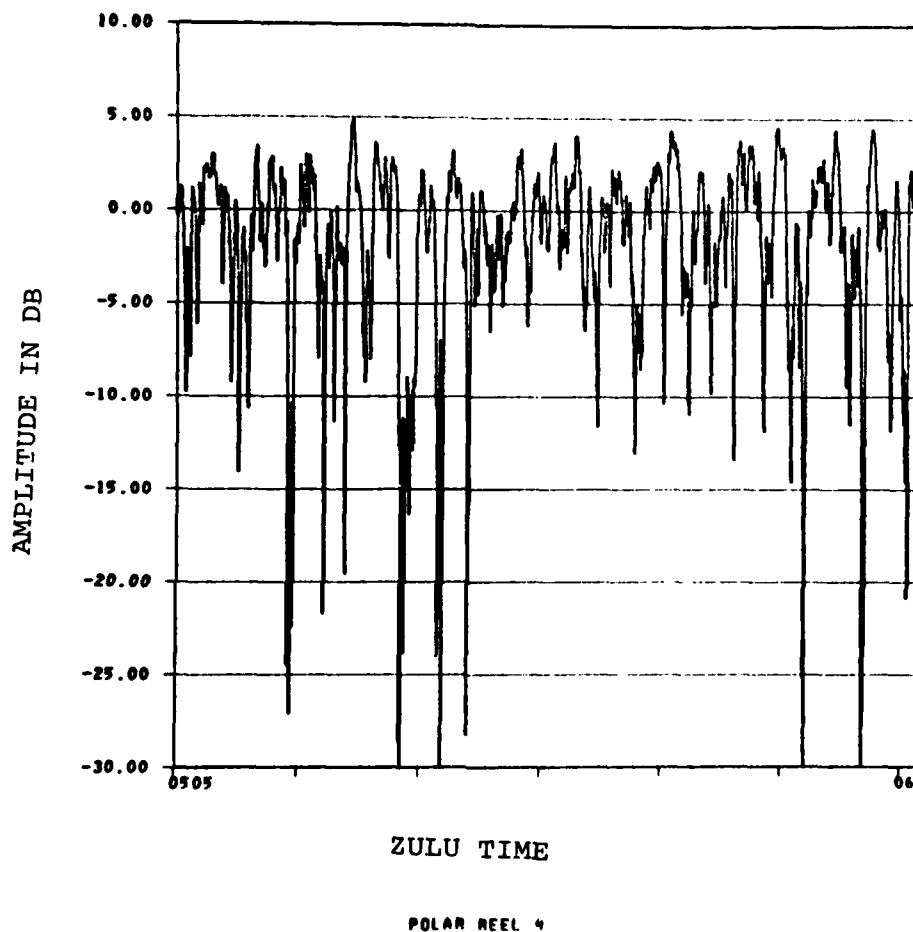
Figure 2-9. Amplitude of SDS UHF signal observed during strong fading in the 26 January 1979 polar flight test.
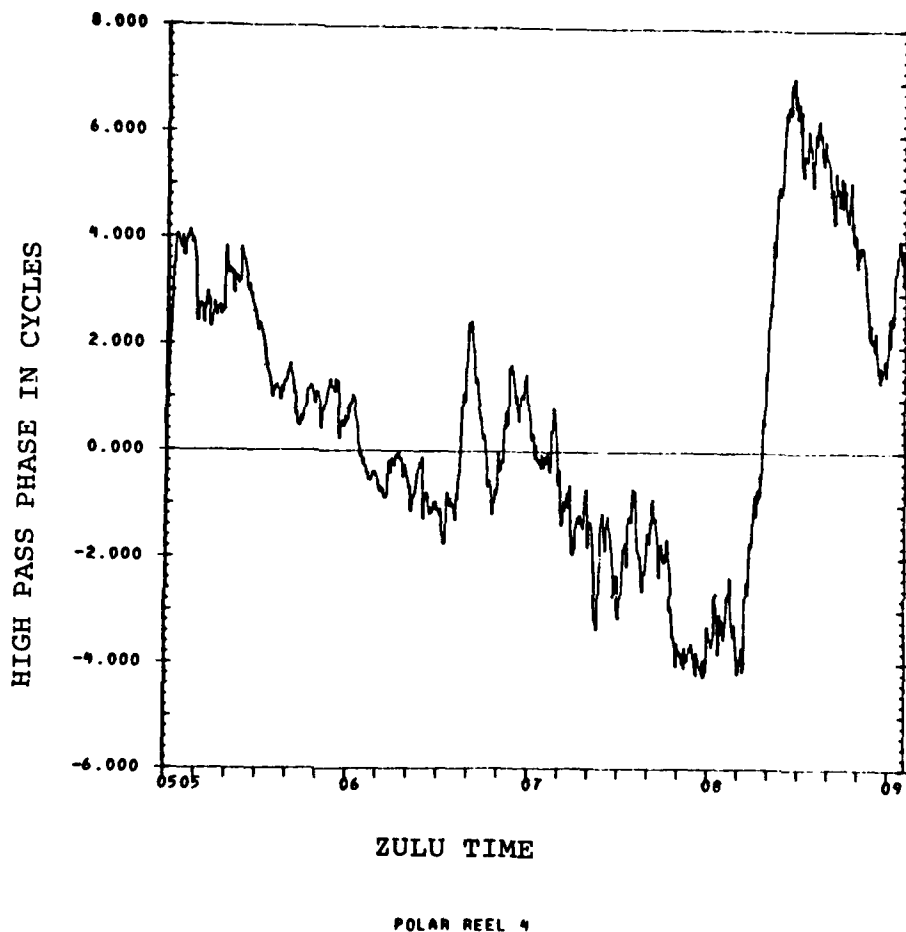
Figure 2-10. Phase of SDS UHF signal observed during strong fading in the 26 January 1979 polar flight test.

26

are available (examples include Fremouw, et al., 1978, Ref. 8, J. Aarons, et al., 1977, Ref. 11, and K.C. Yeh, et al., 1981, Ref. 12). Similar to the polar case the phase measurements have been predominantly performed using the WIDEBAND satellite (however, a work with which the author is unfamiliar by J. Koster, 1978, Ref. 13 which is referenced in K.C. Yeh, et al., Ref. 12, may be exeptional). Thus, the scintillation measurements of FLTSAT signals available from a December 19, 1979 flight test may represent the first equatorial phase measurements from a stationary satellite.

Figures 2-11 and 2-12 display the amplitude and phase of the signal received from FLTSAT during a portion of the flight in which no fading was believed to be present based on strip chart output. The carrier-to-noise ratio, determined from the FLTSAT digital data, is 4 dB less than in the LES-8 data and, consequently, the FLTSAT amplitude fluctuations shown in Figure 2-11 are greater than those in Figure 2-1 for the LES-8 measurements. Note that, in fact, low level scintillations may be present in this data as indicated by the lower frequency fluctuations in the data most apparent near 0354:10. In spite of this fact, the phase fluctuations of Figure 2-12 are believed to be a good indication of the phase stability available, especially because its fluctuations are comparable to those of LES-8 (Figure 2-2) and SDS (Figure 2-8).

The effects of strong equatorial fading are shown in Figures 2-13 and 2-14 and they resemble the strong polar fading seen in Figures 2-9 and 2-10. The amplitude plot in Figure 2-13 shows fade depths to 29 dB and focuses to nearly 5 dB. The first twenty seconds shows fading with

ZULU TIME

FLT-SAT FILE 2
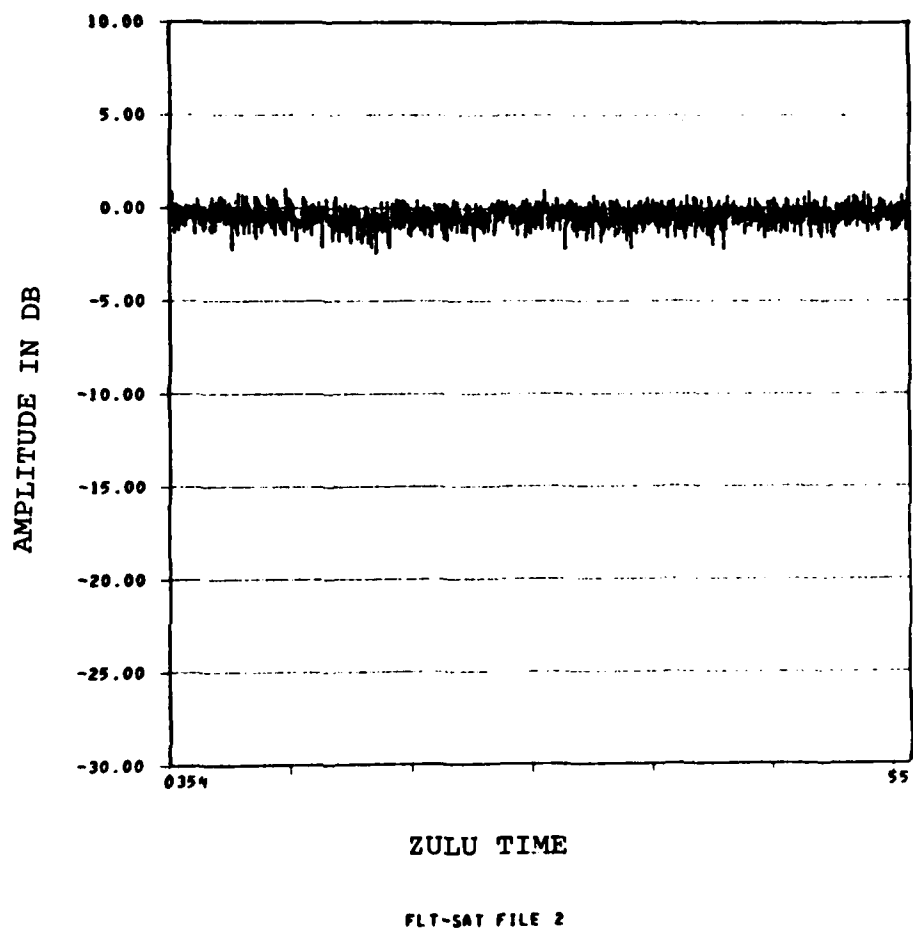
Figure 2-11. Amplitude of the FLTSAT UHF signal
observed during a quiet portion of
the 19 December 1979 flight test near
the geomagnetic equator.

28
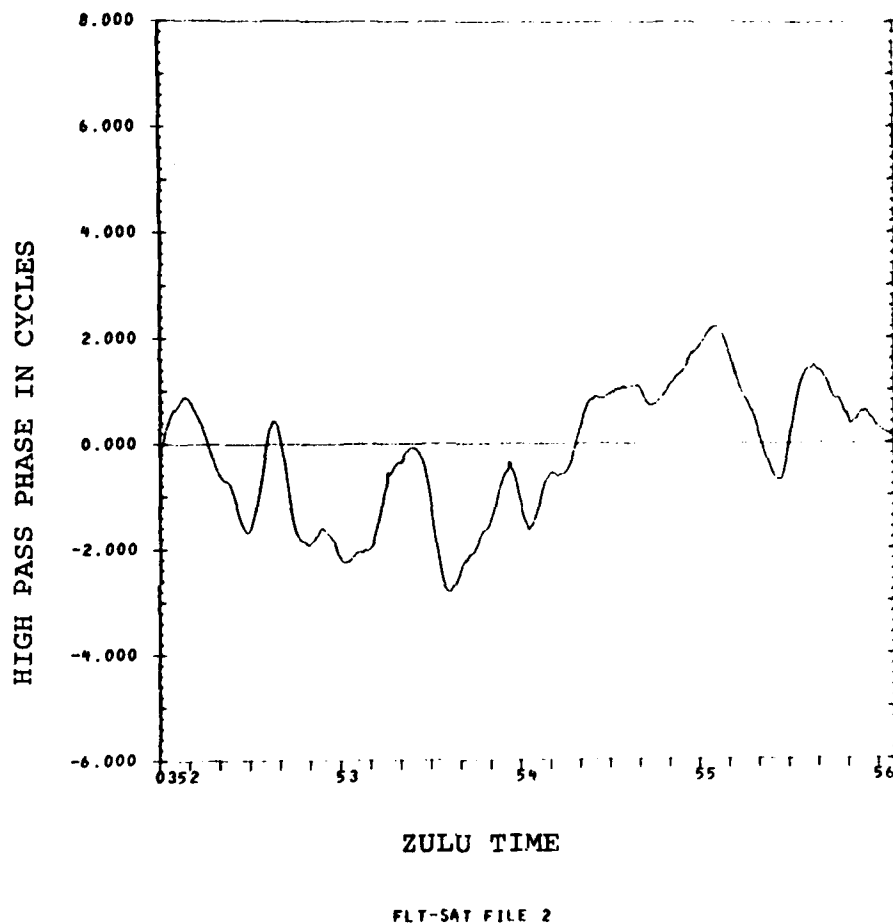
Figure 2-12. Phase of the FLTSAT UHF signal observed during a quiet portion of the 19 December 1979 flight test near the geomagnetic equator.

29
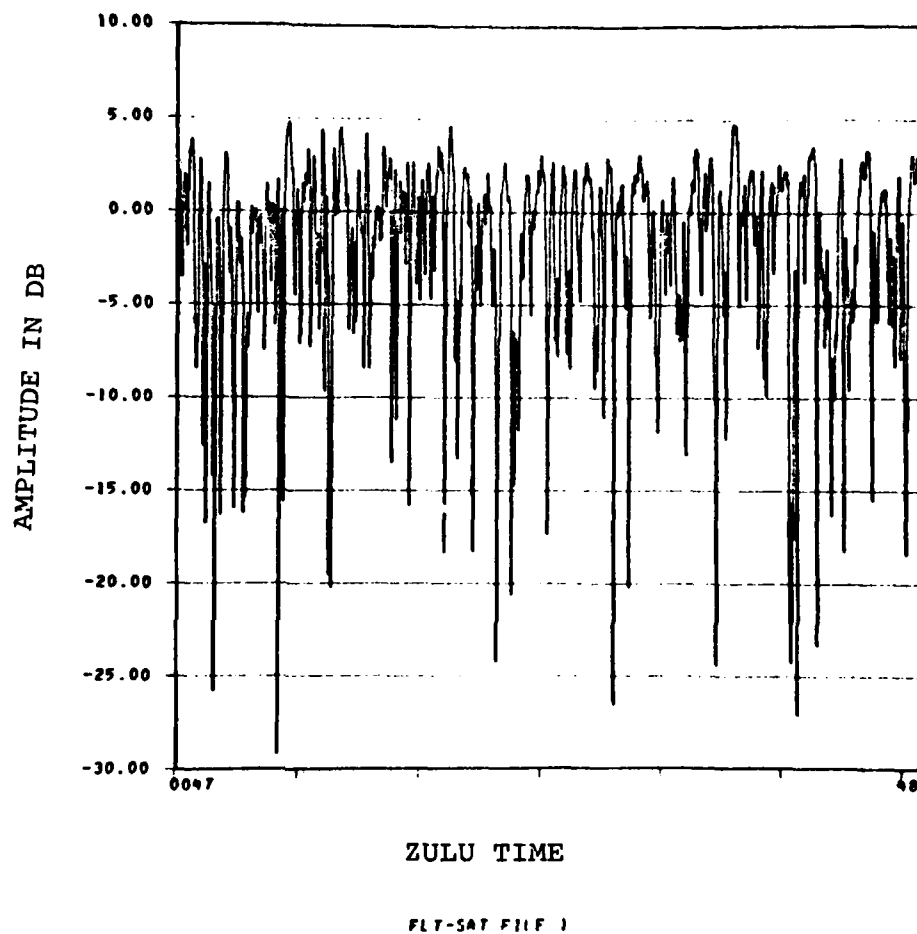
Figure 2-13. Amplitude of the FLTSAT UHF signal during strong fading observed in the 19 December 1979 flight test near the geomagnetic equator.

30

ZULU TIME

FLT-SAT FILE I
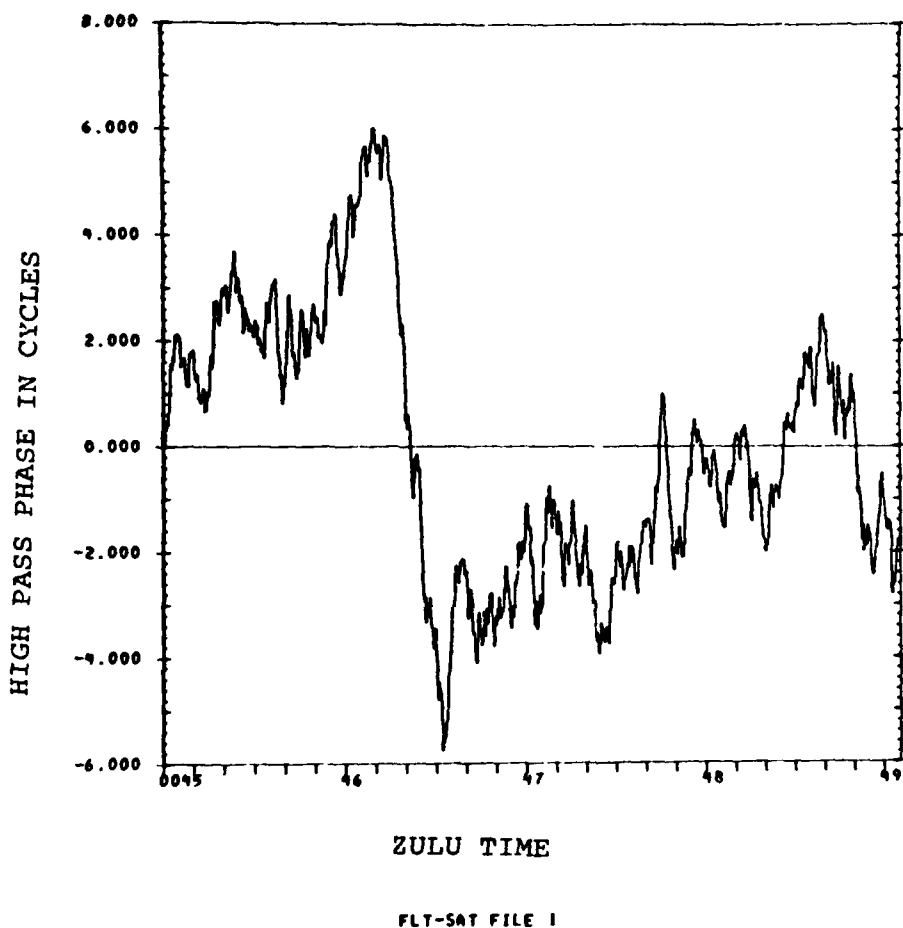
Figure 2-14. Phase of the FLTSAT UHF signal during strong fading observed in the 19 December 1979 flight test near the geomagnetic equator.

31

rates that exceed those in the polar fading amplitude plot. The phase plot in Figure 2-14 shows a structure that is very similar to that of the polar scintillation phase effects seen in Figure 2-10. Numerous slope discontinuities are evident. The nature of these discontinuities is quantified in Chapter 3.

2-5   PERU BARIUM MEASUREMENTS

In March of 1979 the Max Planck Institute performed the CASTOR equatorial barium cloud experiment. The experiment was an attempt to generate an ionospheric bubble and equatorial spread-F through the interaction of the electric fields generated between two ionized barium clouds. The barium clouds were created by barium releases at a planned altitude of 275 kilometers with a separation of 50 km (Johnson and Swanson, 1979, Ref. 14). During the experiment the 662 aircraft measured signals from LES-8 and LES-9 to find evidence of ionospheric irregularities. The LES-9 data has been made available for processing in order to find indications of barium induced phase effects.

Measurements of barium cloud amplitude and phase scintillation effects have been made in the DNA STRESS and PLACES experiments using signals from a stationary satellite (LES-8 and LES-9). These measurements show strong fading effects. The amplitude scintillations are similar to the strong polar and equatorial fading seen in Figures 2-9 and 2-13. The phase effects measured in STRESS show phase fluctuations on the order of tens of cycles for 4-50 minutes after release (Prettie, et al., 1977, Ref. 14). No such effects were observed in the CASTOR data.

Figures 2-15 thru 2-18 show the amplitude and phase from two different portions of the flight. These two portions are separated by a turn in excess of 180°. They therefore traverse similar regions of the sky but in opposite directions.

The carrier-to-noise ratio for this data is 6 dB lower than that of LES-8 of Figure 2-1 and, thus, the amplitude fluctuations due to noise are much more pronounced. The amplitude plot of Figure 2-17 illustrates fluctuations due to noise only. The amplitude plot of Figure 2-15 shows additional fluctuations with a peak-to-peak excursion of about 2 dB.

The phase plotted in Figure 2-16 shows fluctuations with magnitude less than that of LES-8 and FLTSAT. Also visible are a higher frequency fluctuation. This high frequency fluctuation is the result of a phase noise spur at .4 Hz and is not of ionospheric origin. The phase plotted in Figure 2-18 is similar to that of Figure 2-16 with the possible exception of the feature near 0050:40. This feature has a large enough magnitude to be potentially significant, however, the absence of a concurrent amplitude *effect weighs against the possiblility* that it is of barium origin. Over the 450-500 km slant range amplitude effects from a 1 cycle Gaussian with 2 km e-fold phase disturbance should have developed to a detectable level.
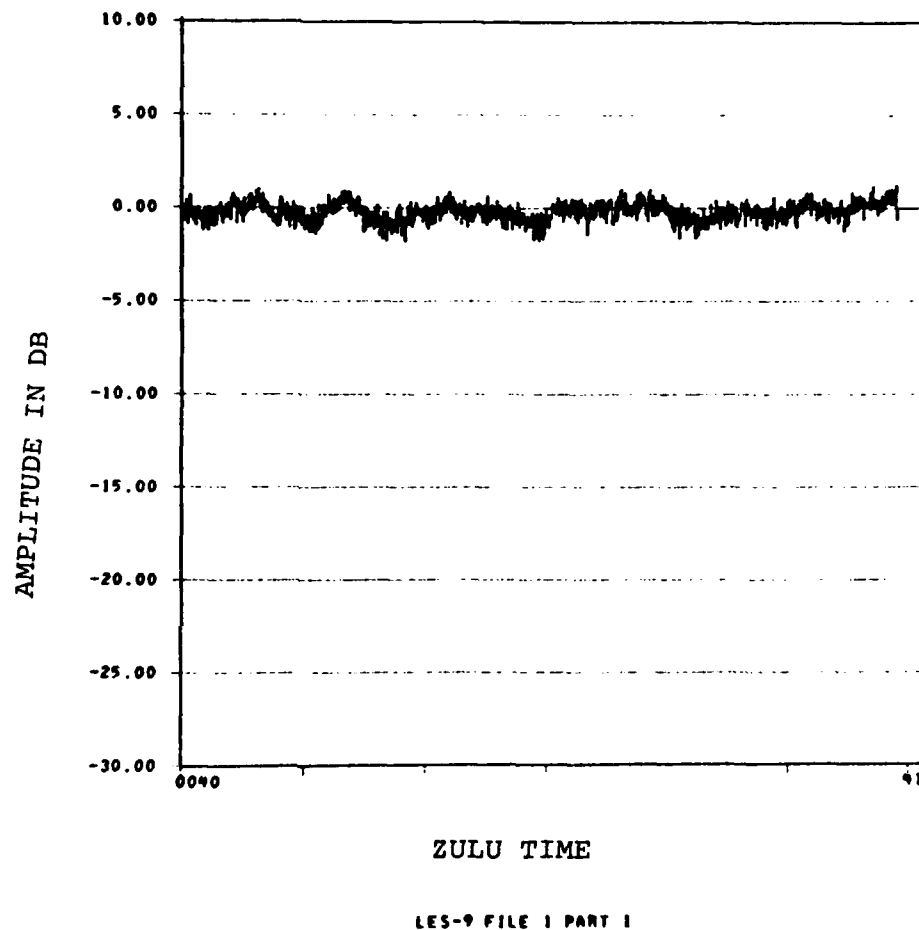
Figure 2-15. Amplitude of the LES-9 UHF signal
             during the first portion of data
             from the CASTOR barium release in
             Peru on 23 March 1979.

34
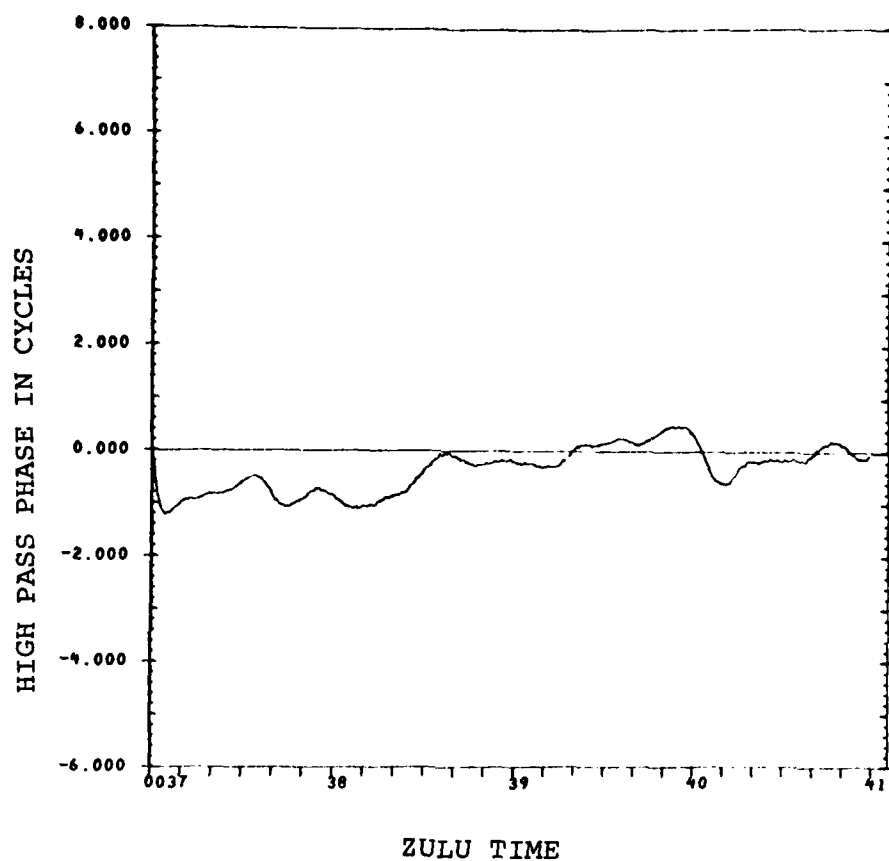
Figure 2-16.   Phase of the LES-9 UHF signal
during the first portion of data
from the CASTOR barium release i:
Peru on 23 March 1979.
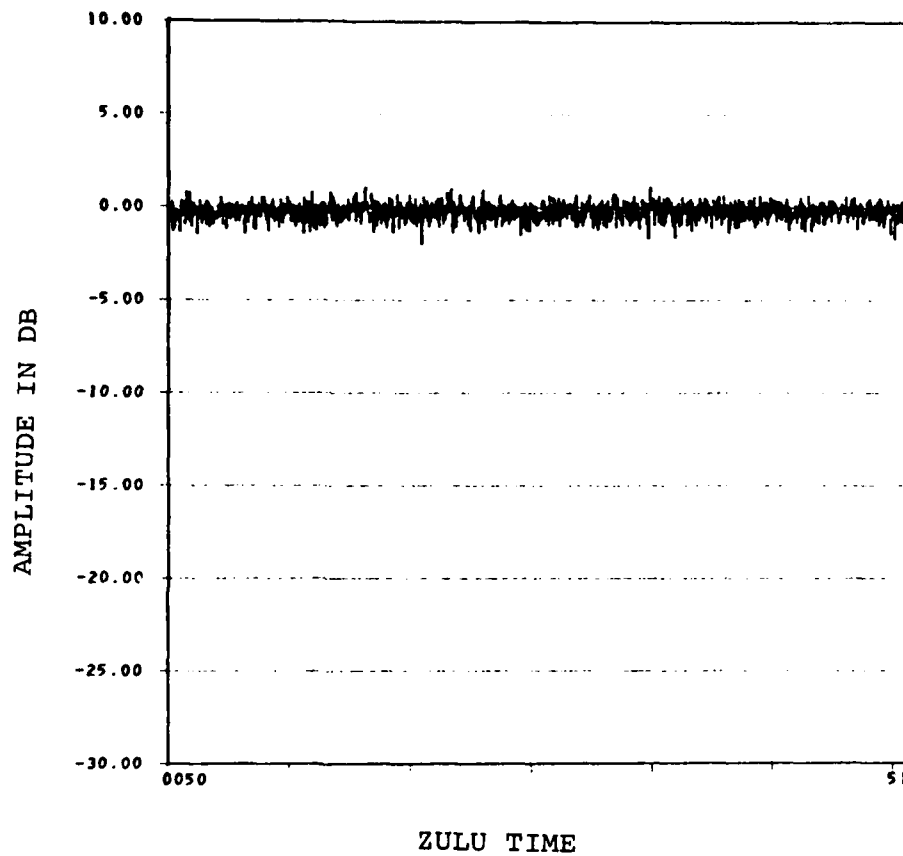
Figure 2-17. Amplitude of the LES-9 UHF signal
during the second portion of data
from the CASTOR barium release in
Peru on 23 March 1979.

36
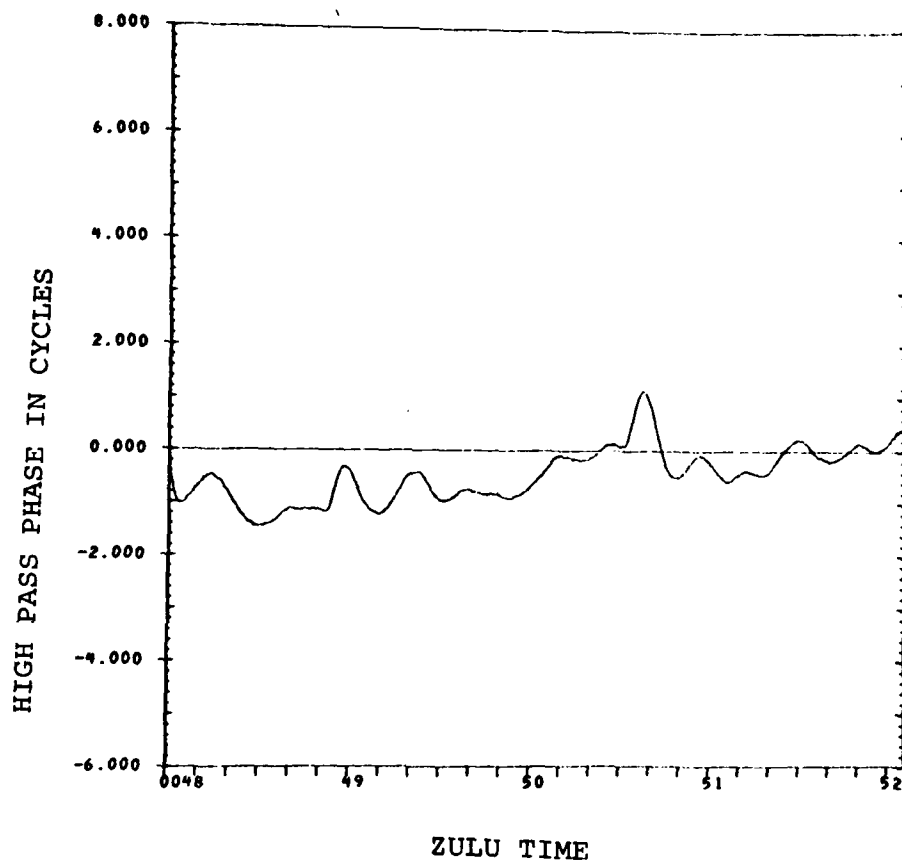
Figure 2-18. Phase of the LES-9 UHF signal
during the second portion of data
from the CASTOR barium release in
Peru on 23 March 1979.

37

SECTION 3

MEASUREMENTS OF PHASE EFFECTS

Section 2 presented numerous displays demonstrating the qualitative nature of the signal phase fluctuations which accompany amplitude scintillations. This section attempts to demonstrate their quantitative nature.

Several quantities are discussed, namely the variance of the phase difference over a specified interval, the power spectral density of the phase, and the probability density of the phase difference. It should be apparent from the phase plots in Section 2 that in referring to phase dependencies the continuous phase is meant and not phase modulo two pi. For the sake of power spectral density measurements the phase is further understood to be referenced to the average frequency over the data interval in question.

3-1 PHASE DIFFERENCE STANDARD DEVIATION

This section presents measurements of the standard deviation of the phase difference over a specified separation interval. This quantity gives a measure of the phase wander by the end of the interval and is thereby a direct measure of the phase stability. Since the phase difference divided by the interval length is the average frequency over the interval this quantity is closely related to the root mean square (r.m.s.) frequency fluctuations. Specifically, the r.m.s. frequency fluctuation is the standard deviation of the phase difference over a specified length divided by that length.

Plots of the standard deviation of phase difference over a separation interval versus the interval length are shown in Figures 3-1 thru 3-9. Figures 3-1 thru 3-3 show the results of the Platteville data, Figures 3-4 and 3-5 show polar data, Figures 3-6 and 3-7 show equatorial data, and 3-8 and 3-9 show Peru barium data.

As an example of one of the plots consider Figure 3-1 which shows LES-8 data from the quiet portion of the April 16, 1980 flight test. It shows a monotonically increasing dependence on the phase difference interval starting from a standard deviation of 3.5° over .01 seconds. This lowest value reflects, to a large extent, the system signal-to-noise ratio although large scale fluctuations do influence it. Note that for an ideally stable carrier in a high carrier-to-noise ratio situation the curve would become constant over time intervals longer than the inverse system bandwidth (30 Hz for all data herein—a 2-pole complex low pass filter with 15 Hz 3 dB breakpoint was used for all processing presented herein). The presence of phase instability is evidenced by the lack of such behavior. In order to construct the plot, standard deviations were calculated at phase difference values at the .01 second basic sampling interval and at all the possible octaves of .01 second. To expedite calculation, samples of phase differences over a given interval are taken at the rate of two phase difference samples per given interval; for example, every 1.28 seconds the phase difference over 2.56 seconds is calculated and entered into the calculation of the standard deviation. Note that the standard deviations at very large difference intervals are less reliable because they have been
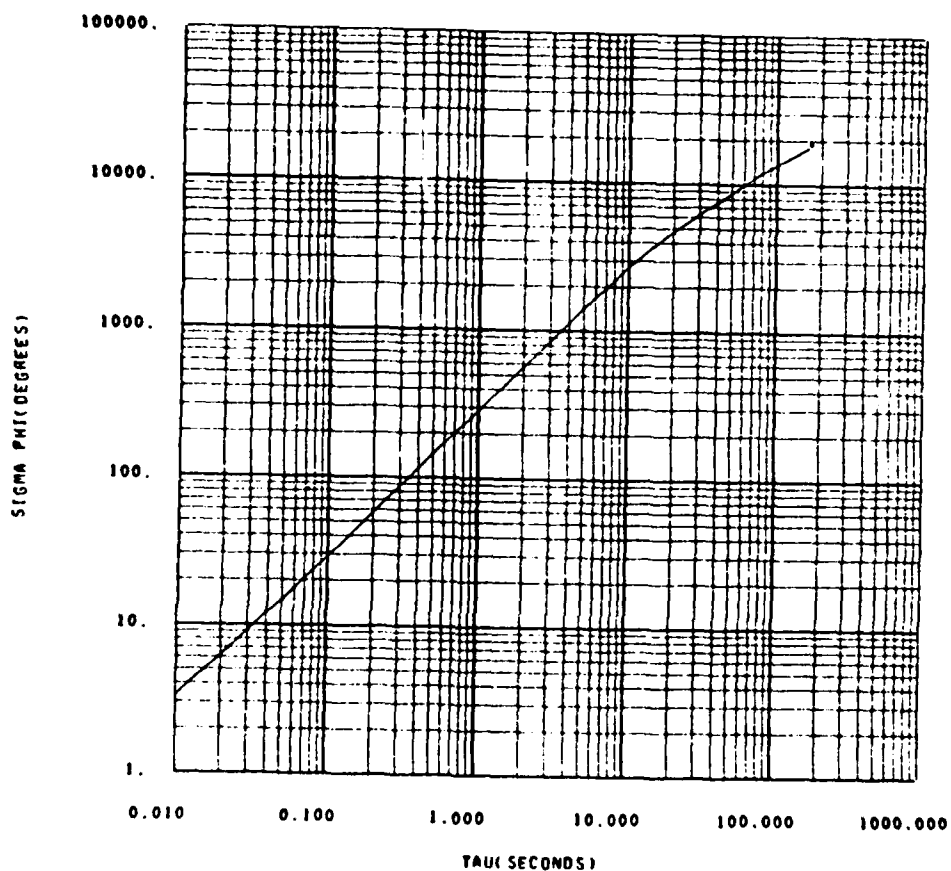
Figure 3-1. LES-8 phase difference standard deviation over differencing interval of length tau versus tau for the quiet portion of the April 16, 1980 Platteville flight test.

40
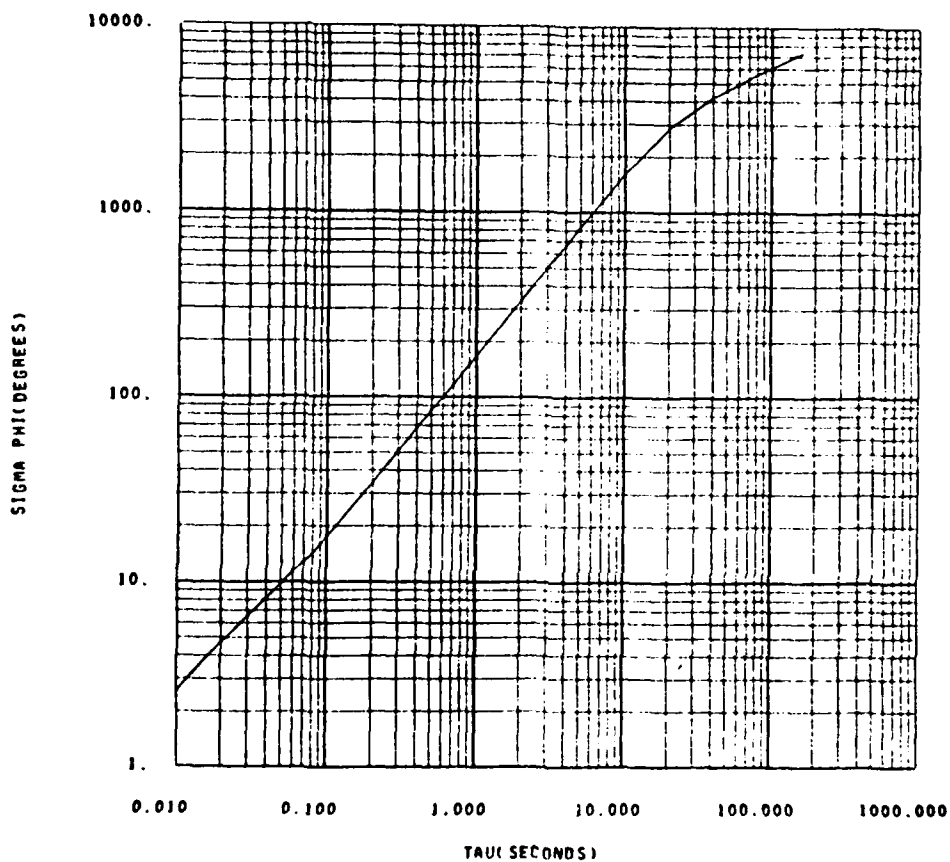
Figure 3-2. LES-9 phase difference standard
deviation over differencing interval
of length tau versus tau for
Platteville overdense heating.
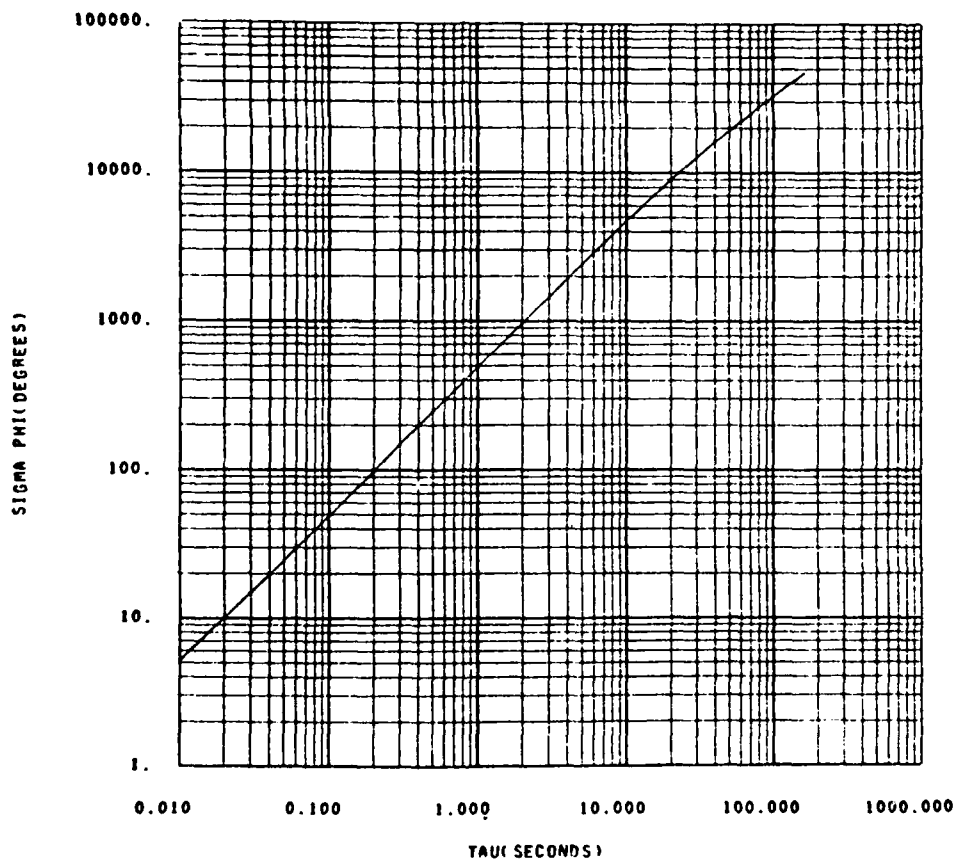
Figure 3-3. LES-8 phase difference standard deviation over differencing interval of length tau versus tau for Platteville underdense heating.
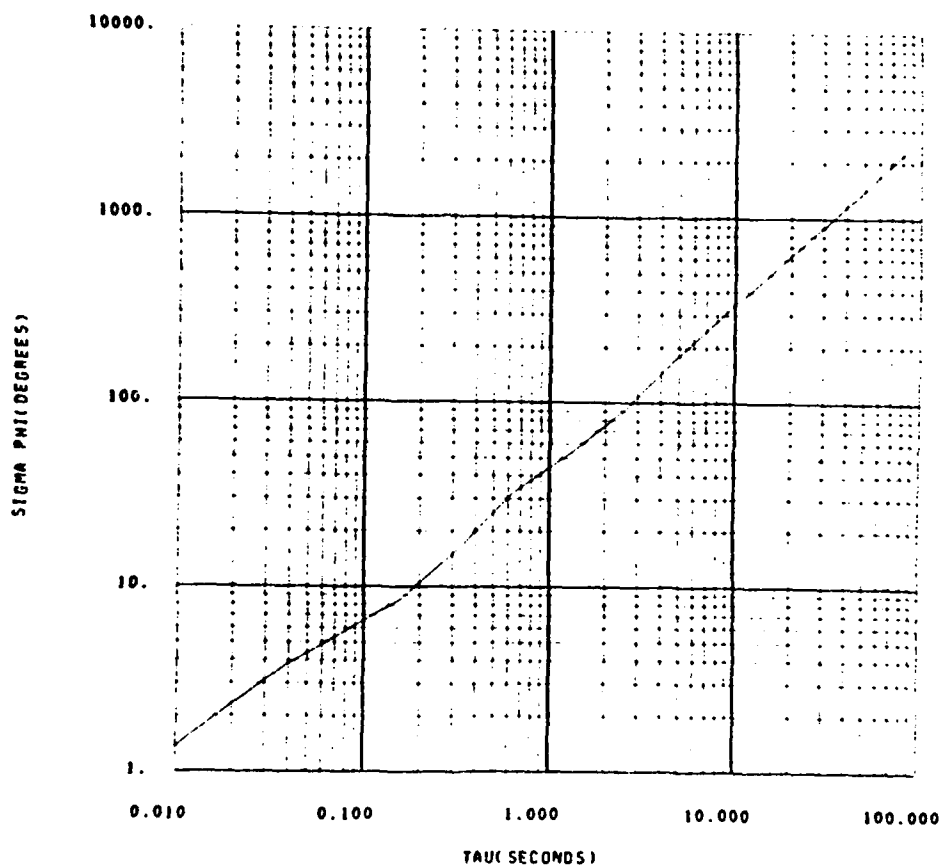
Figure 3-4. SDS phase difference standard deviation over differencing interval of length tau versus tau for the weak fading portion of the 26 January 1979 polar flight test.
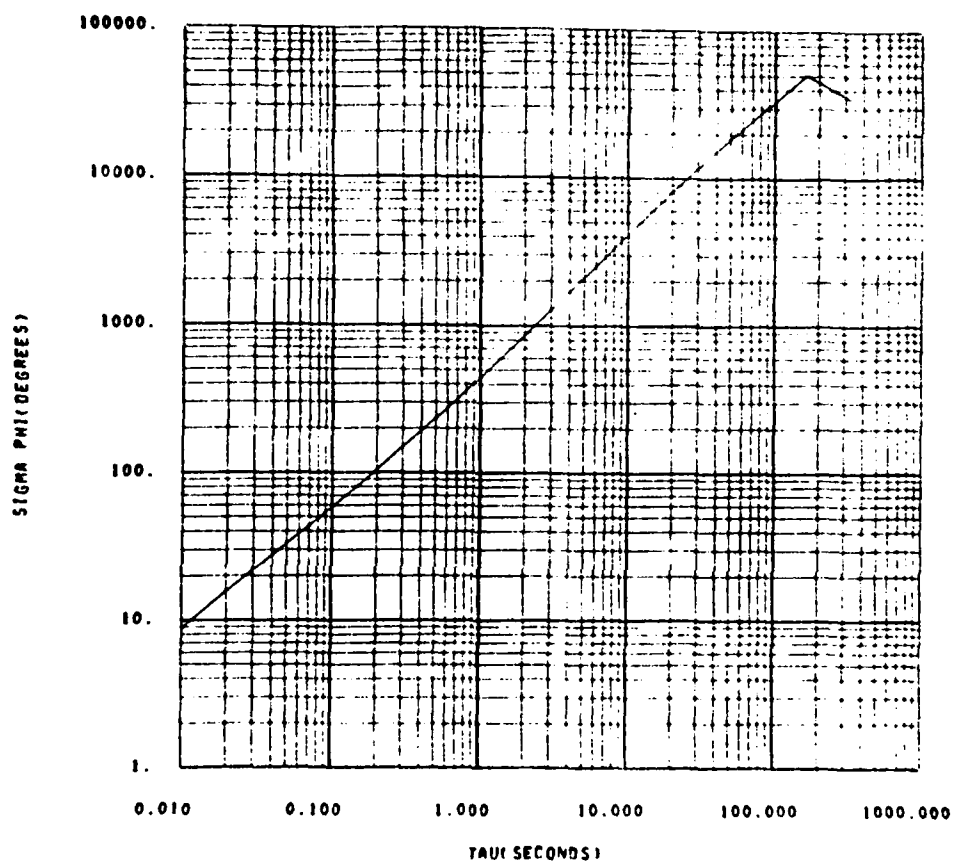
Figure 3-5. SDS phase difference standard
deviation over differencing interval
of length tau versus tau for the
strong fading portion of the 26 January
1979 polar flight test.

44
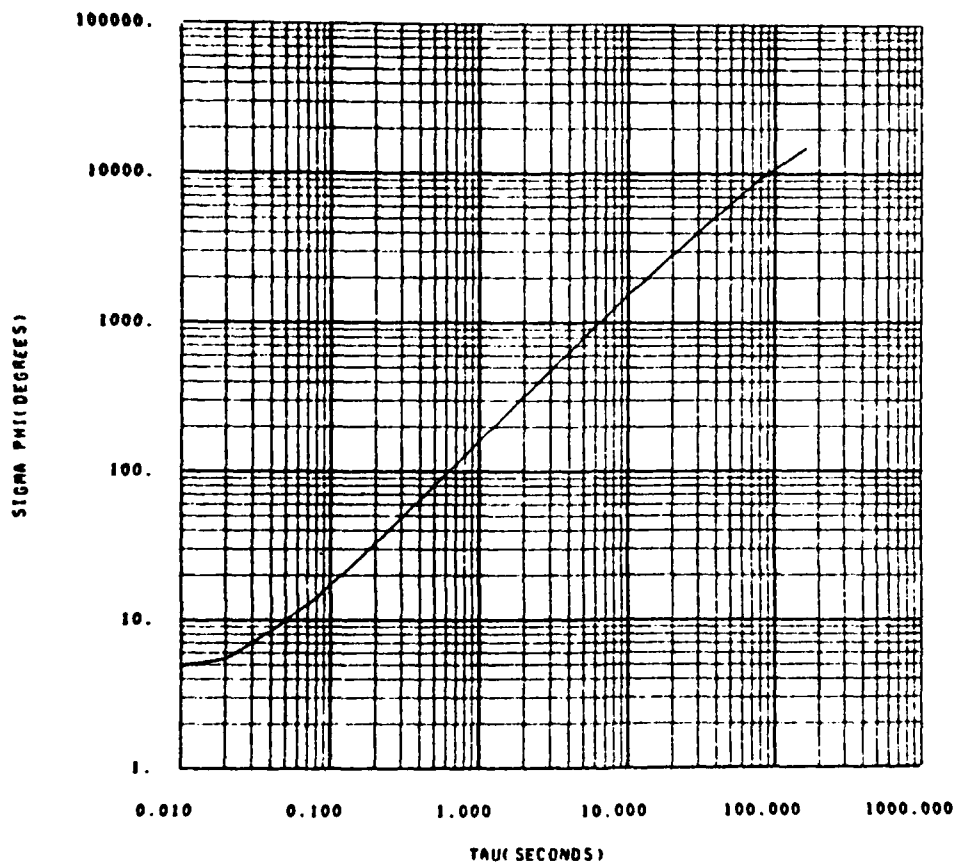
Figure 3-6.   FLTSAT phase difference standard
              deviation over differencing interval
              of length tau versus tau for the
              quiet portion of the 19 December 1979
              equatorial flight test.
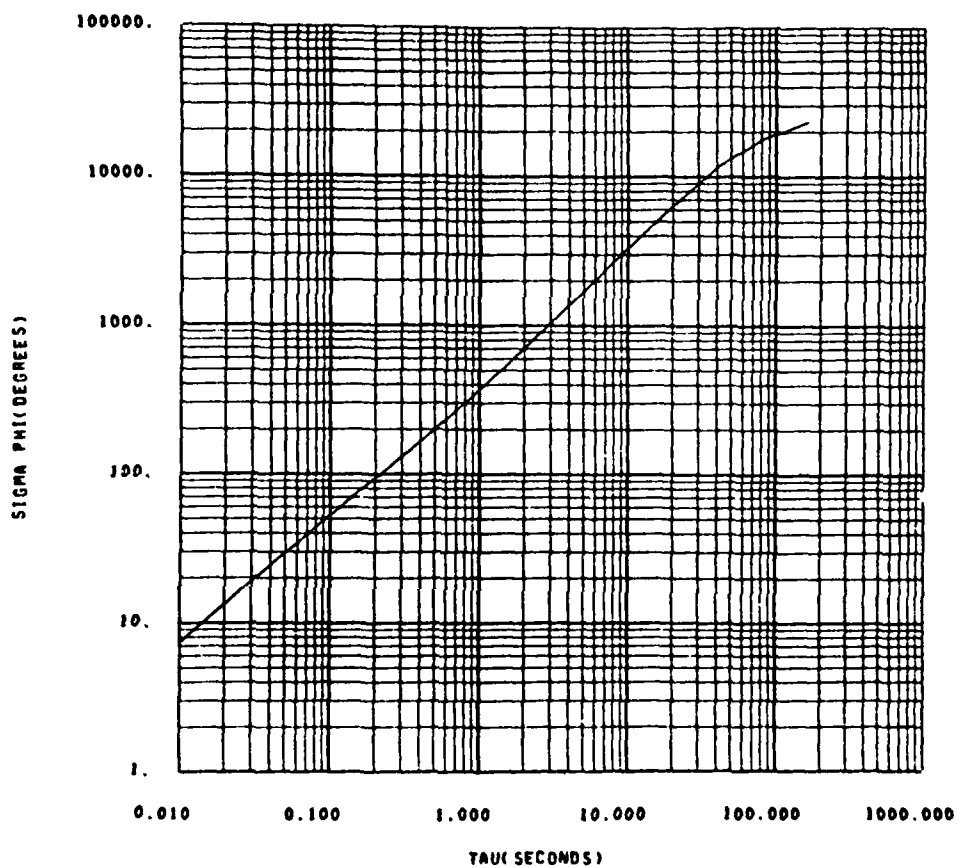
Figure 3-7. FLTSAT phase difference standard
deviation over differencing interval
of length tau versus tau for the
strong fading portion of the
26 January 1979 equatorial flight test.

46
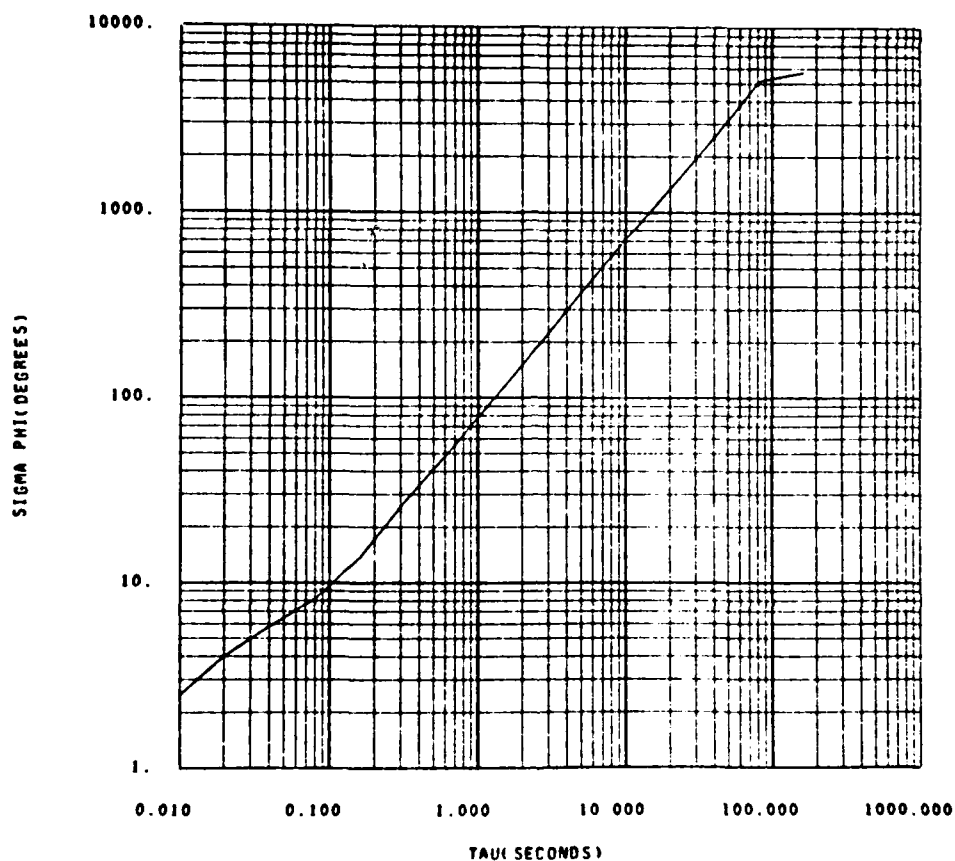
Figure 3-8. LES-9 phase difference standard deviation over differencing interval of length tau versus tau for the first portion of data from the 23 March 1979 Peru barium (CASTOR) flight test.

47
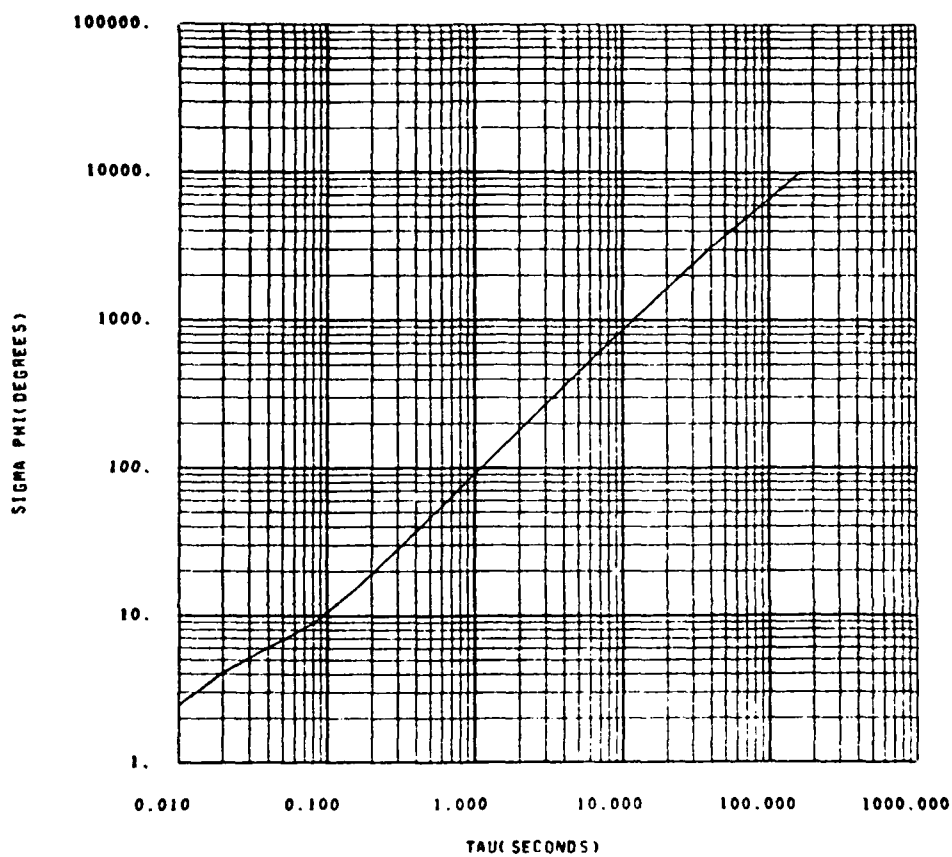
Figure 3-9. LES-9 phase difference standard
deviation over differencing interval
of length tau versus tau for the
second portion of data from the
23 March 1979 Peru barium (CASTOR)
flight test.

48

derived from fewer samples. Data derived from fewer than
four samples have not been plotted.

Figure 3-2 shows LES-9 Platteville phase standard
deviation data for overdense heating conditions. Surprisingly,
the data has less phase variance than the LES-8 data of
Figure 3-1 at all difference interval values. (Note that
the ordinate scale has one less decade than that of Figure
3-1.) The ionospheric variations induced by overdense
Platteville fading are apparently unresolvable at the phase
noise level of LES-8. However, LES-9 data is typically less
noisy than LES-8 data. A comparison of Figure 3-2 with
Figures 3-8 and 3-9, the phase standard deviation from the
two portions of the Peru barium data, shows that phase
fluctuations associated with ionospheric heating are
represented in Figure 3-2 between .02 and 50 seconds.

Figure 3-3 shows LES-8 phase standard deviation for
the case of Platteville underdense heating. A significant
increase in this quantity above the reference curve of
Figure 3-1 is observable. It can also be observed that phase
fluctuations due to underdense heating are significantly
larger than those due to overdense heating.

Figures 3-4 and 3-5 show the phase difference standard
deviation behavior for SDS polar weakly fading and strongly
fading data, respectively. Figure 3-4 indicates a phase
stability from SDS that is significantly better than that
from LES-8 and comparable to or better than that from LES-9.
The phase deviation data for the strong fading situation
shows, in Figure 3-5, much larger values than the phase
stability reference of Figure 3-4. Phase fluctuations due
to fading are seen to have a standard deviation greater than
one cycle over a 1 second interval.

49

Figures 3-6 and 3-7 show FLTSAT phase standard
deviation data for quiet and strongly fading environments.
The FLTSAT phase stability available appears to lie between
that of LES-8 and LES-9 and is more than adequate to
reveal the phase effects of strong fading seen in Figure
3-7. Figure 3-7 shows a phase difference standard deviation
of approximately one cycle over a one second interval.

Figures 3-8 and 3-9 illustrate the phase standard
deviations for the first and second portion of data from
the Peru barium flight. As noted in Section 2-5, the second
portion demonstrates slightly more phase activity than the
first. This observation is quantified by these plots which
show the second portion greater by a factor of about 1.2.

Table 3-1 gives a tabulation of the values of phase
difference standard deviation over 1 second and 10 second
intervals for ease of comparison. An important point to
note in comparing data is that the standard deviation at
a fixed difference interval will increase slowly with
increasing processing lengths. Figure 3-10 shows the results
of processing a one minute length of Platteville overdense
data in place of the six minute length used to derive the
results of Figure 3-2. The phase standard deviation
increased by a factor of about 1.6 with this factor of six
increase in processing length. In this respect it should
be noted that all of the processing intervals are 6 to 8
minutes long--and thus mutually comparable--with the execption
of the SDS weak fading data which is only 3 minutes long.

Table 3-1. Standard deviation of phase difference

| Satellite	Fading	Situation	$\sigma_{\Delta\phi}$ in degrees	
			1 sec	10 sec
SDS	strong	polar measurements	450	4,200
FLTSAT	strong	equatorial measurements	360	3,300
LES-8	weak	Platteville underdense	480	4,800
LES-9	weak	Platteville overdense	160	1,600
LES-9	weak	Peru barium first portion	75	710
LES-9	weak	Peru barium second portion	90	850
LES-8	quiet	Platteville flight	280	2,700
FLTSAT	quiet	equatorial flight	160	1,500
SDS	weak	polar flight	45	350
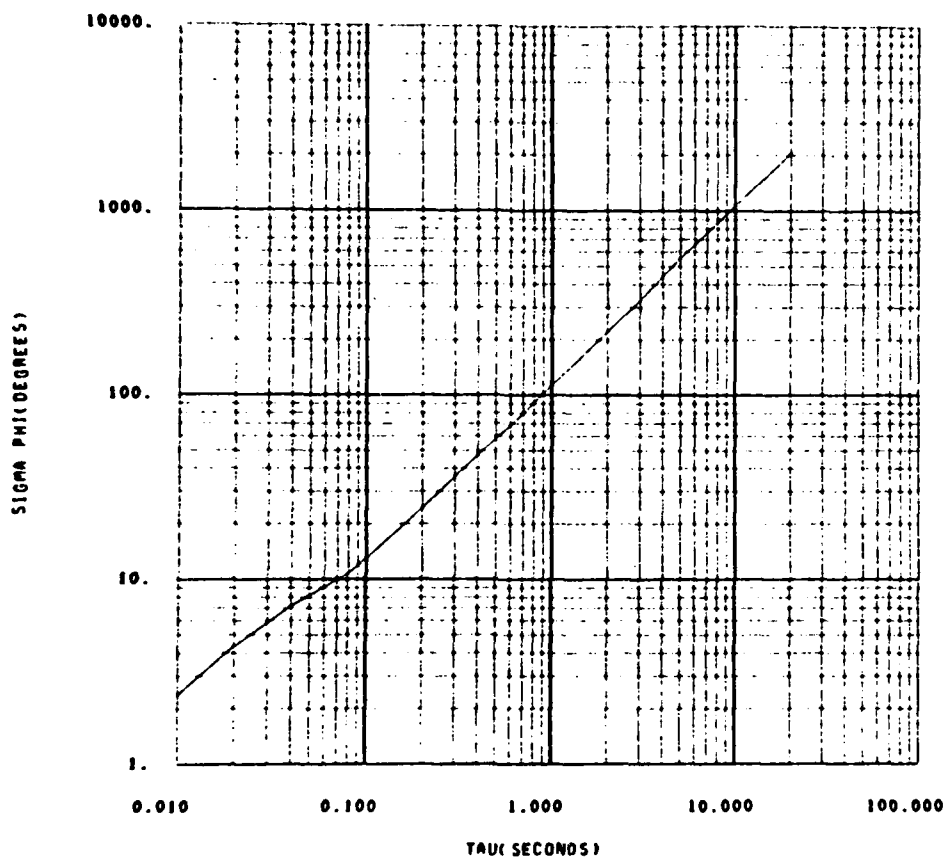
Figure 3-10. LES-9 phase difference standard deviation over differencing interval of length tau versus tau for a one minute portion of the Platteville overdense heating data. A comparison with the data of Figure 3-2 demonstrates the slight increase in phase standard deviation with a six-fold increase in the interval of data processed.

52

3-2   PHASE POWER SPECTRA

The phase power spectral density is another measure
of phase fluctuations which is useful for identifying
harmonics in the data and for examining the underlying
physical processes that produced the data. Figure 3-11
shows four plots which illustrate the phase power spectra
obtained from the AFWAL data and their mutual relationships.
Each of the four plots is a set of smoothed spectra over-
layed for comparison with a color key given by data file.
The correspondence between data file and data source is
given in Table 3-2 along with the start and end time of
the data segment used for spectral analysis.

The upper left plot of Figure 3-11 shows the power
spectral density of phase data from Platteville measurements.
The data taken during underdense heating labelled as LES-8
File 2 has values larger than any of the other situations
at frequencies less than .2Hz. Beyond .2 Hz the data taken
during overdense heating shown as LES-9 File 2 dominates.
The high frequency overdense data has a spectral roll-off of
about 20 dB per decade beyond .4 Hz. This roll-off is
characteristic of phase fluctuations which are associated
with moderate to strong amplitude fluctuations. The under-
dense phase spectral density at frequencies below .2 Hz is
larger than the reference phase spectral density of LES-8
File 1 by 4 to 5 dB. In this same frequency regime the
overdense data is less than or equal to this LES-8 phase
reference, consequently the data of LES-9 File 1 Part 1 is
shown as a LES-9 phase reference. Comparison of the two
LES-9 spectral data files shows that the overdense data
could be the result of ionospheric effects down to frequencies
as low as .002 Hz. On the other hand, however, both the
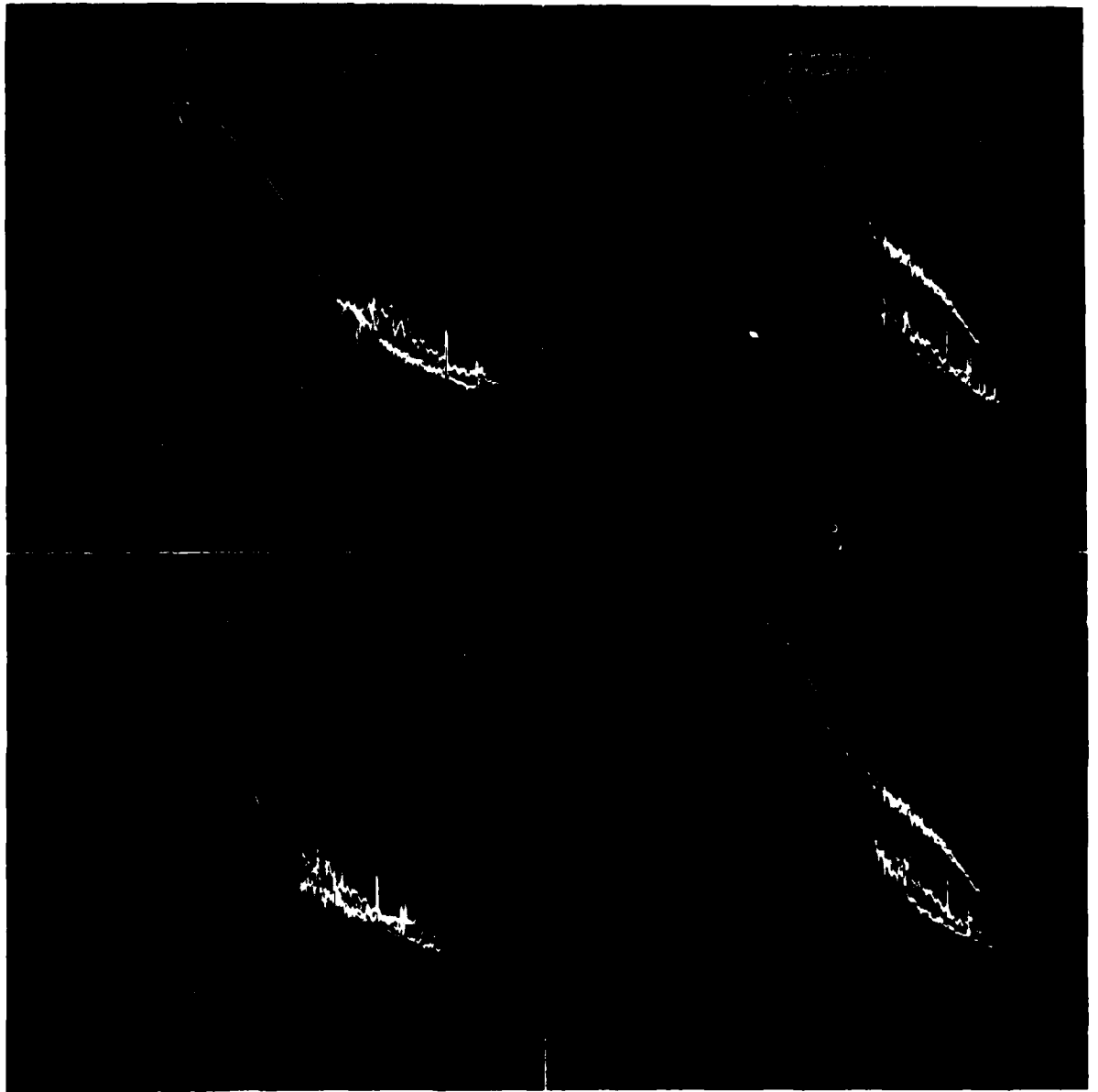
Figure 3-11. Phase spectral densities for
AFWAL data files.

Table 3-2. Data files for spectral analysis

File Name	Measurement	Interval Processed
FLTSAT File 1	Equatorial fading	0044:00 – 50:05
FLTSAT File 2	Equatorial quiet	0349:57 – 58:02
LES-8 File 1	Platteville quiet	0141:58 – 48:03
LES-8 File 2	Platteville underdense	0247:59 – 54:04
LES-9 File 1 Part 1	Peru barium	0031:00 – 37:05
LES-9 File 1 Part 2	Peru barium	0047:00 – 53:05
LES-9 File 2	Platteville overdense	0201:46 – 07:01
Polar Reel 4	SDS strong fading	0504:00 – 14:00
Polar Reel 2	SDS weak fading	0325:00 – 28:05

underdense phase power spectrum and the overdense phase power spectrum have steeper slopes with higher frequencies. The phase reference data from LES-8 File 1 also illustrates the same behavior and this fact could point to a common origin of artifact with variable magnitude, such as aircraft dynamics.

The upper right plot of Figure 3-11 shows comparisons of the phase spectra from the strong fading equatorial and polar data, labelled as FLTSAT File 1 and Polar Reel 4, respectively. The two curves are closely matched down to a frequency of .01 Hz. From .1 Hz to 2 Hz the density curves roll-off at the typical 20 dB per decade. Also shown on the plot are the equatorial and polar phase spectral density reference plots labelled FLTSAT File 2 and Polar Reel 2, respectively. The strong fading equatorial data is very close to its no fading reference in the frequency range of .02 to .05 Hz. In contrast, the weak fading polar data lies significantly below the polar curve at all comparable frequencies. The polar reference curve also lies significantly below the FLTSAT reference curve at frequencies below 1 Hz. Thus, unless it can be shown that one to two order of magnitude differences in aircraft dynamics existed between the polar reference data and numerous other files, aircraft dynamics can be ruled out as a source of artifact in all but the polar reference data.

The plot in the lower left portion of Figure 3-11 shows a comparison of the first and second portions of the Peru barium flight labelled LES-9 File 1 and LES-9 File 2, respectively. From .006 Hz to .2 Hz the spectrum of the second portion is from 0 dB to 5 dB higher than the spectrum of the first portion. While this fact may suggest the

presence of ionospheric disturbances it should be noted
that if disturbances are present they are small as indicated
by a comparison with quiet (!) data from LES-8. Also shown
is the weakly fading polar data. The disturbances must be
so small that the phase effects from polar weak fading
dominate them beyond .1 Hz.

The plot in the lower right of Figure 3-11 shows a
comparison of all files that demonstrate ionospheric phase
effects (with a high likelihood) against the weak fading
polar data which itself probably demonstrates ionospheric
fading effects beyond .1 Hz. The strong fading polar and
equatorial data are especially prominent at frequencies
beyond .1 Hz. Perhaps surprisingly, the phase fluctuations
from underdense heating in LES-8 File 2 are comparable to
or greater than these strong fading environments from .009
to .07 Hz.

All the plots of Figure 3-11 show strong harmonics
at $2.^{+}$ Hz, $4.^{+}$ Hz and $6.^{-}$ Hz. Because of the universality
of these harmonics they must be artifact which originates
in the receiving, recording, reproducing, or digitizing
processes. The spectra from files of LES-9 data also
illustrate further harmonics of .4 Hz. These harmonics
are probably due to satellite phase noise.

The spectra were generated using the sine transform
and not the conventional discrete Fourier transform. The
piece-wise linear segments of the plot are generated with
a maximum likelihood estimator for a power law fit. The
sine transform is discussed in Appendix A and the maximum
likelihood estimator in Appendix B.

57

3-3   HISTOGRAMS OF PHASE DIFFERENCE

Formats such as BPSK are frequently considered for
use in satellite communications links. An understanding of
the effects of the phase perturbations associated with
strong fading is necessary to predict their performance
through a disturbed ionosphere. It would be reasonable for
a systems designer making an analysis of BPSK to consider
the phase degradation over a bit decision interval to be
the combination of fading phase effects and noise induced
phase effects. It might be tempting to assume that the total
phase wander over a bit decision is Gaussian distributed
with a variance equal to the sum of the noise induced phase
variance and the fading induced phase variance (the latter
as shown in Section 3-1) and to, thereby, allow evaluation
of a probability of error integral. Such an evaluation would,
however, produce erroneous results because of the non-Gaussian
nature of the phase perturbations associated with fading. The
purpose of this section is to display this non-Gaussian nature
as observed in the AFWAL data and to specify relations that
quantify their nature and impact.

Figures 3-12 through 3-20 illustrate histograms of
the phase difference over three different interval lengths
for the strong fading observed in the equator and polar
flight tests and for the case of relatively little phase
activity as observed during the first portion of the Peru
barium flight test. Also shown on each curve is a Gaussian
with equivalent first and second moments. The data is
displayed for differencing intervals of .01, .16, and 1.28
seconds. For a 75 bit per second BPSK system the phase
difference curves for the .01 second interval would be most
relevant.
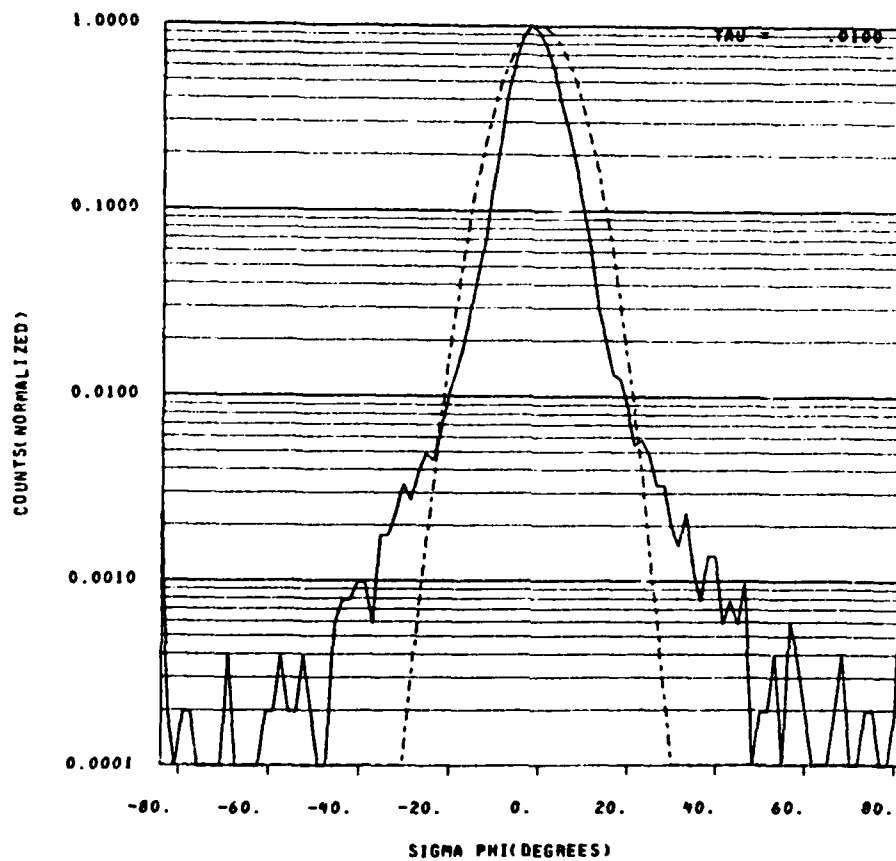
Figure 3-12. Histogram of phase difference of FLTSAT signal over a .01 second difference interval during strong equatorial fading.
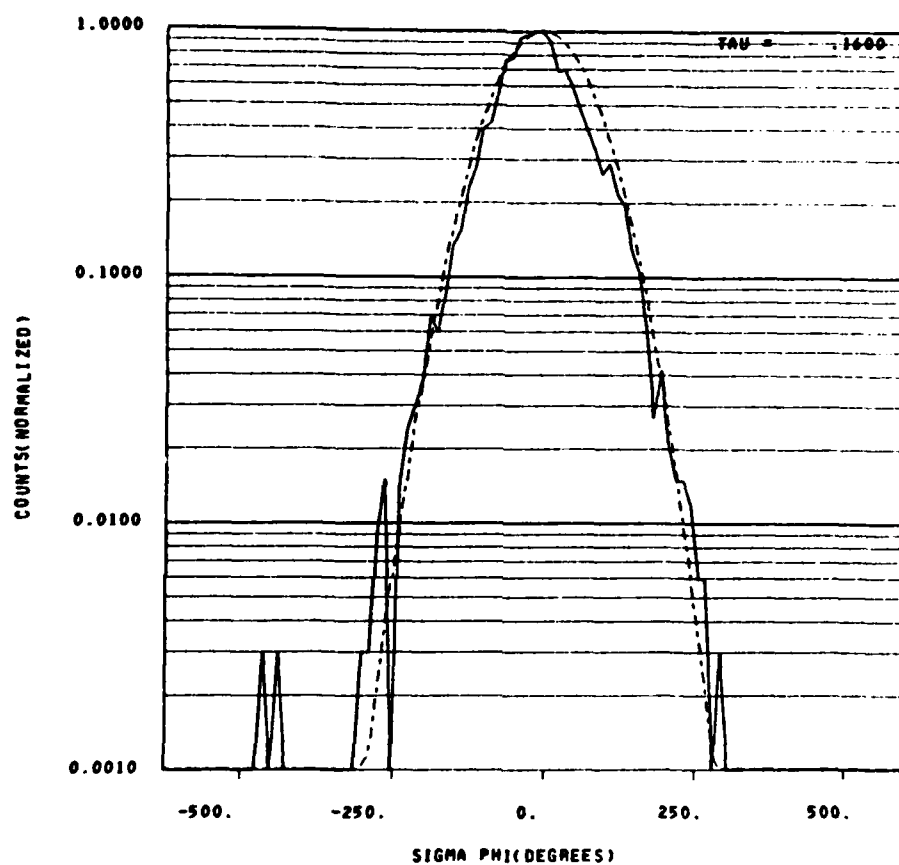
Figure 3-13. Histogram of phase difference of FLTSAT signal over a .16 second difference interval during strong equatorial fading.

60
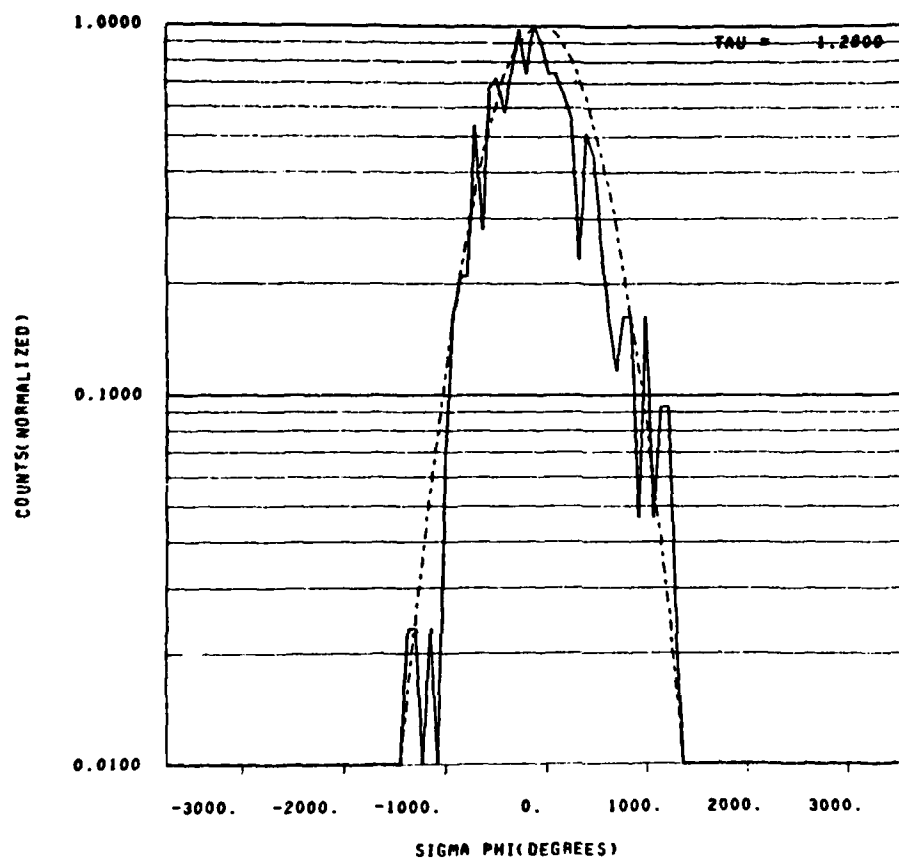
Figure 3-14. Histogram of phase difference of
FLTSAT signal over a 1.28 second
difference interval during strong
equatorial fading.

61
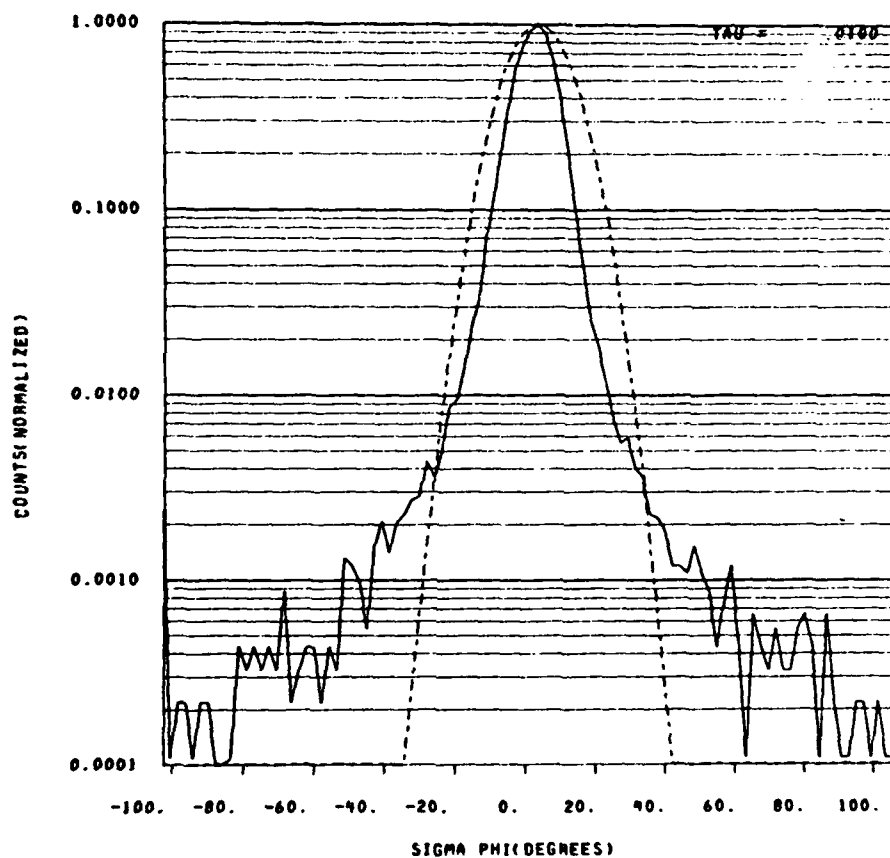
Figure 3-15. Histogram of phase difference of SDS signal over a .01 second difference interval during strong polar fading.
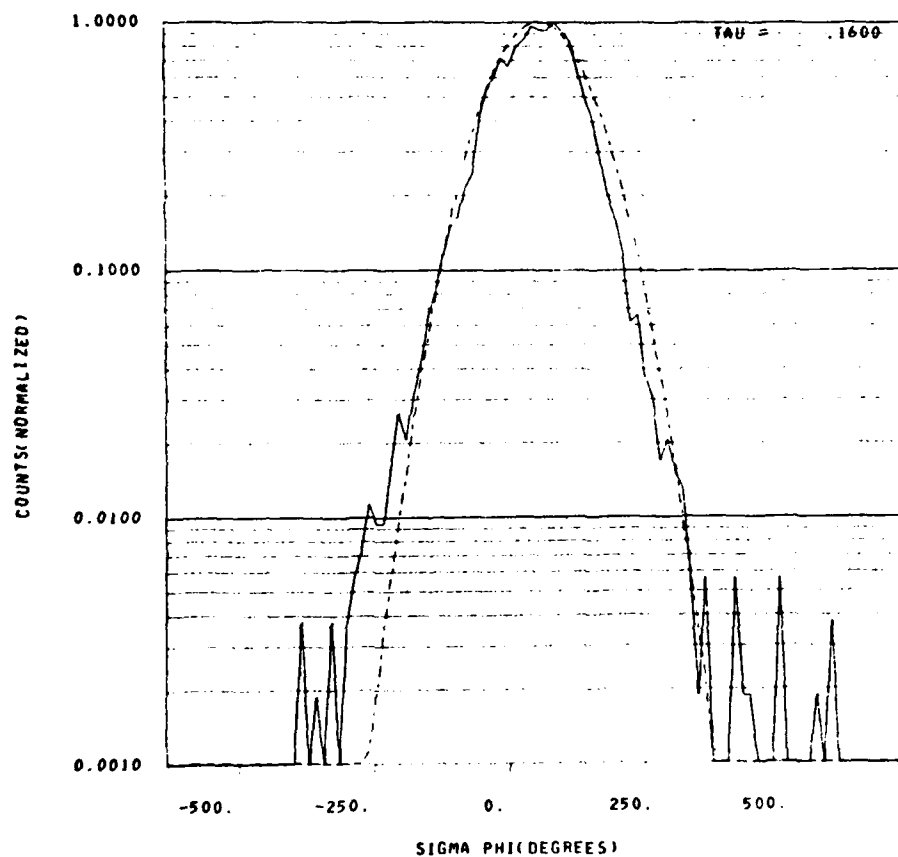
Figure 3-16. Histogram of phase difference of SDS
signal over a .16 second difference
interval during strong polar fading.

63
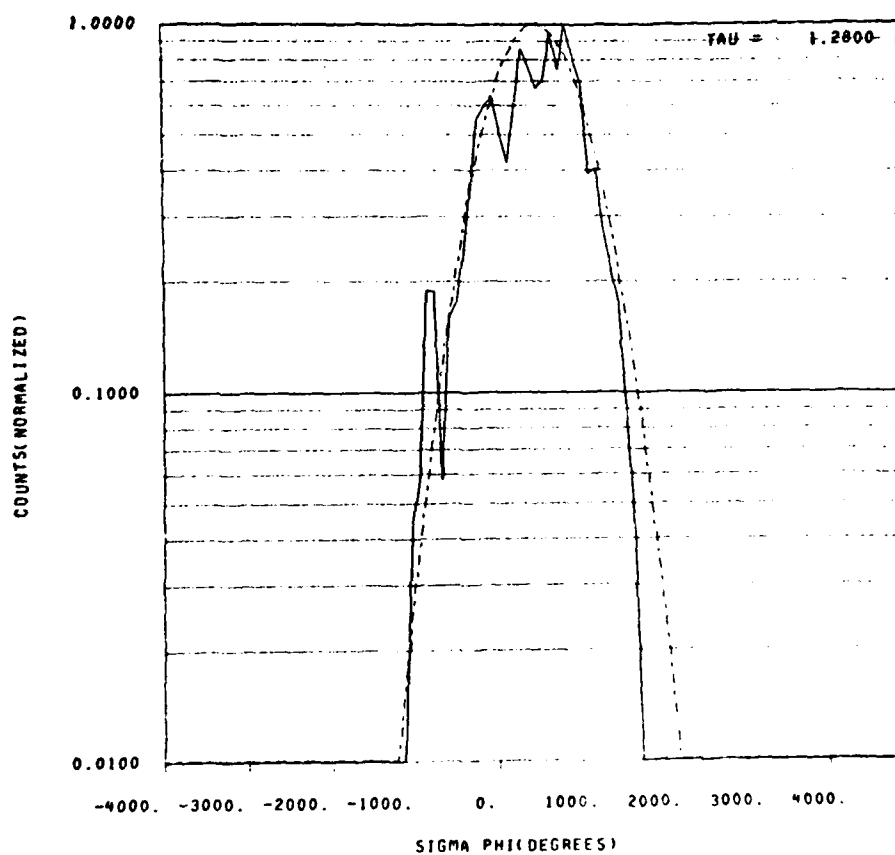
Figure 3-17. Histogram of phase difference of SDS
signal over a 1.28 second difference
interval during strong polar fading.
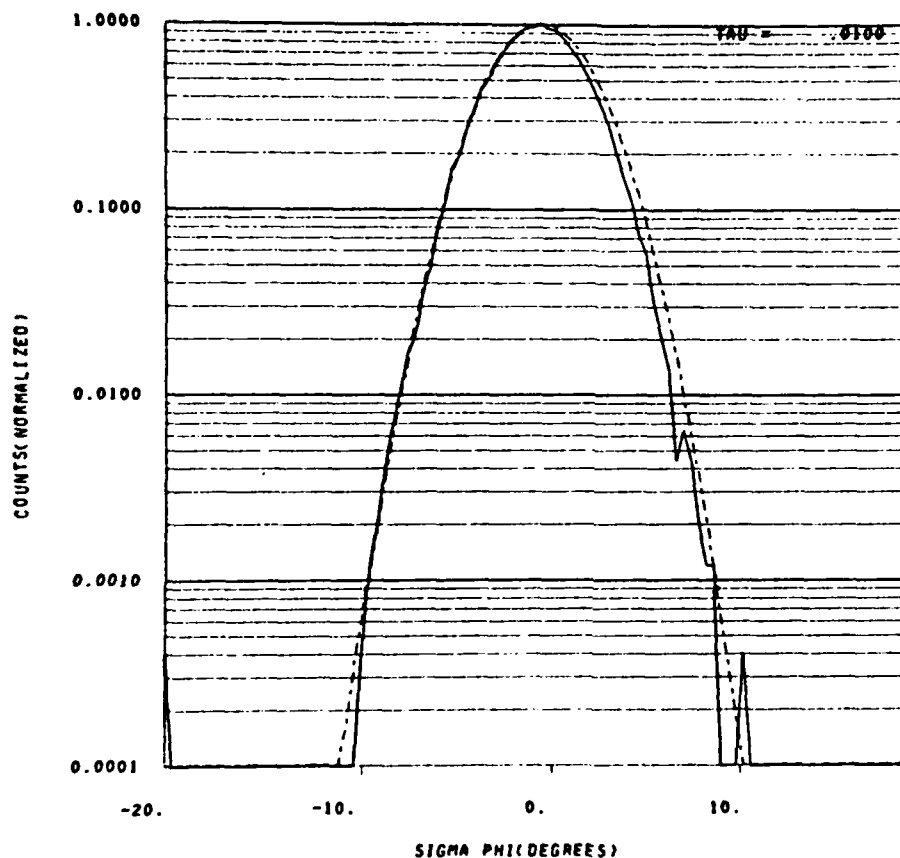
Figure 3-18. Histogram of phase difference of LES-9 signal over a .01 second difference interval shown as a quiet reference. Data is from the first portion of the Peru barium flight test.

65
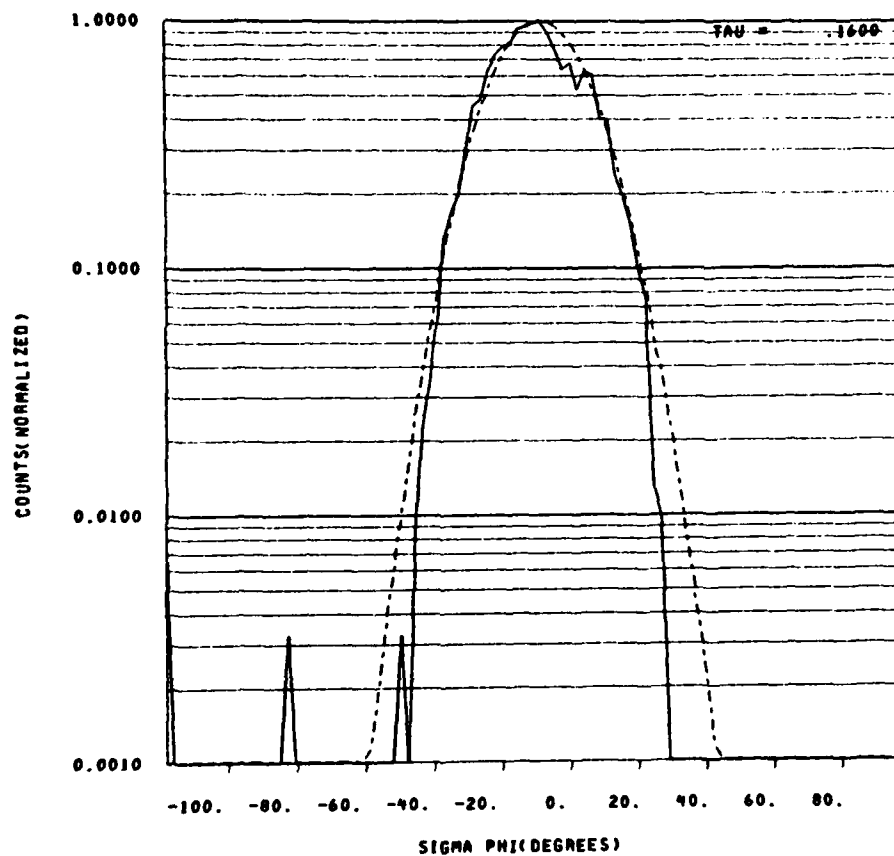
Figure 3-19. Histogram of phase difference of LES-9 signal over a .16 second difference interval shown as a quiet reference.

66
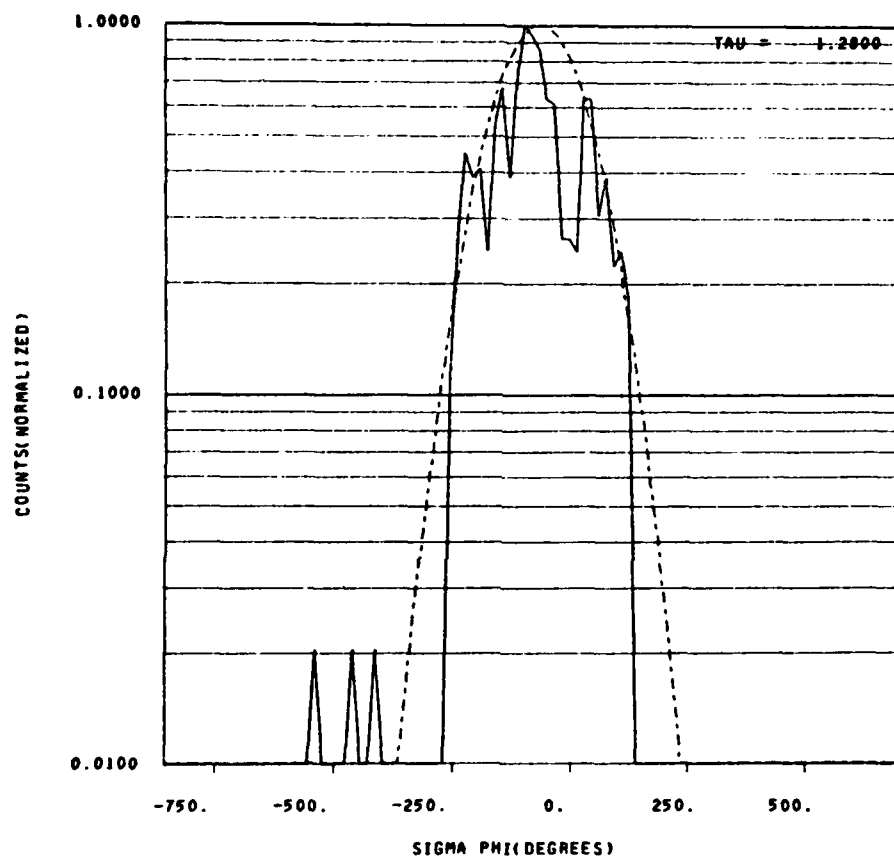
Figure 3-20. Histogram of phase difference of LES-9 signal over a 1.28 second difference interval shown as a quiet reference.

The non-Gaussian nature of the phase difference over the .01 second differencing interval is readily apparent in Figures 3-12 and 3-15. Note that the abscissa scales of these two plots are expanded to a range of 12 standard deviations on either side of the mean. The enhanced values at the two extremes of these plots represent the count of points lying beyond the 12 standard deviation limits. Note that a 75 bit per second BPSK system requires that the phase difference not exceed 67.5 degrees in .01 second to avoid an irreducible error rate, i.e., an error rate that cannot be reduced through the use of increased power. Errors of this type would exist in both the polar and equatorial environments.

As the difference interval length is increased the phase difference histograms become more closely approximated by Gaussian fits as illustrated in Figures 3-13 and 3-14 for the equatorial data and in Figures 3-16 and 3-17 for the polar data. There is less data over the longer difference intervals and, thus, the deviations from the fits become more pronounced, however, the general trend toward Gaussian convergence is evident. For comparison with a record of little or no phase activity the corresponding data from the first portion of the Peru barium flight test is shown in Figures 3-18 thru 3-20.

The behavior of the phase difference over the .01 second interval emphasizes the resemblance between strong fading and a weak c.w. signal in narrowband Gaussian noise. The strong fading first order amplitude distribution has a well-known resemblance to that of a weak c.w. signal in narrowband Gaussian noise. As the fading becomes very strong its amplitude tends toward a Rayleigh distribution which is also the amplitude distribution for the limiting case of

68

narrowband noise only. S.O. Rice (1945 and 1948, Ref. 16 and 17) has extensively analyzed the properties of a c.w. signal in random noise. In Reference 17 he develops expressions for the distribution of instantaneous frequency. For the limiting case of narrowband noise only the probability density of instantaneous frequency in Hz, f, is given as

$$p(f) = \frac{1}{2B} \frac{1}{(1 + (f/B)^2)^{3/2}}$$

where B is the r.m.s. bandwidth of the noise process and is defined by

$$B^2 = \frac{\int_0^\infty f^2 S(f) \, df}{\int_0^\infty S(f) \, df}$$

and where S(f) is the power spectrum of the complex envelope of the noise process. At larger values of instantaneous frequency the density has a dependence accouding to $|f|^{-3}$, a dependence which closely describes that observed in the histograms of Figures 3-12 and 3-15. Manual fits to the equatorial data below normalized count values of .01 indicate a dependence according to $|f|^{-3.1}$. A similar fit to the polar data produced a dependence according to $|f|^{-2.6}$. The accuracy of the index of these data is approximated as ±.3.

The strong similarity between the histograms and the instantaneous frequency of narrowband noise suggests that for practical purposes the short term fluctuations of strong fading can be considered equivalent to those of narrowband noise.

Assuming that the relation given above holds at the .001 normalized count level an indication of the r.m.s. bandwidth of the signal can be straightforwardly obtained by reading the plot. At this level the polar data has a 54° deviation and the equatorial data has a 40° deviation. These correspond to instantaneous frequencies of 15 Hz and 11 Hz, respectively. Since the .001 count level corresponds to a frequency deviation ten times the r.m.s. bandwidth, r.m.s. bandwidths of 1.5 Hz for the polar and 1.1 Hz for the equatorial data can be inferred.

It may be of interest to note the dependence of the irreducible error rate upon the r.m.s. signal bandwidth. The density of instantaneous frequency may be integrated to give

$$\Pr \{|f| > f_1\} = 1 - (1 + (B/f_1)^2)^{1/2}$$

which for small r.m.s. bandwidths is well approximated by:

$$\Pr \{|f| > f_1\} = \frac{1}{2}\left(\frac{B}{f_1}\right)^2$$

BPSK errors occur when the phase shift exceeds 90° in the bit interval. For a bit interval of T a good approximation to the irreducible error rate is given by:

$$P_{ei} = 8(BT)^2$$

For the polar and equatorial environments, BPSK error rates of 3.2×10^{-3} and 1.7×10^{-3}, respectively, would be expected.

A similar expression can be given for a QPSK link which errors when the phase shift exceeds 45° over the symbol duration. For this case the probability of a symbol error P_e is closely approximated by

$$P_e = 32(BT_s)^2$$

70

where T_s is the symbol period. The irreducible bit error rate for QPSK in terms of the bit interval T_b can also be approximated using similar techniques by

$$P_{be} = 8(1 + \frac{1}{9})(BT_b)^2 .$$

These relations stress the importance of the non-Gaussian nature of the phase fluctuations which is clearly demonstrated in the AFWAL data.

SECTION 4

PHASE MEASUREMENT IMPLICATIONS

Because the primary purpose of the AFWAL flight
tests was the measurement of ionospheric structure and its
effects, the thrust of this section is the discussion of
the inferrences which can be made about structure from
the phase data. The AFWAL phase measurements also bear
implications for other topics such as aircraft flight
dynamics. A brief discussion is also given of that topic.

Phase fluctuations generally reflect fluctuations of
total electron content (TEC) along the line-of-sight. For
the case of an ideal phase reference, i.e., no aircraft
dynamics effects and ideal reception and transmission, the
phase is directly proportional to the TEC. For the 250 MHz
data of this report the constant of proportionality is 1
cycle of phase shift for every 1.87×10^{15} electrons per
square meter along the line-of-sight. The presence of
amplitude fading indicates a distortion in the proportionality
relationship. If the fading is strong the distortion will
exist in all the spectral components of the fluctuations with
large enhancements in the high frequency component strengths.
If the amplitude fading is weak the magnitude of the low-
frequency spectral components may be preserved; however, the
higher frequency components will probably be distorted and
enhanced.

Backpropagation (Prettie, et al., 1977, Ref. 14) can
potentially remove the distortion associated with amplitude
fading if the propagation geometry and the phase stability
meet certain requirements. Backpropagation was attempted
on the Platteville, polar, and equatorial fading data with
little to no success. Results are discussed later in the
appropriate sub-sections.

4-1   PLATTEVILLE HEATER IRREGULARITIES

The phase data from the AFWAL signal measurements suggest two hypotheses. The first is that underdense heating produces irregularities that are larger in magnitude than those produced by overdense heating. The second is that the irregularities produced by underdense heating are larger in size. The irregularity size produced by underdense heating appears to be 3-6 km. Further, the sizes produced by overdense heating appears to be significantly smaller than the approximate lower limit of the dominant overdense structure sizes quoted as 500 meters by Duncan (1981, Ref. 3).

The basic evidence for the first hypothesis is a comparison between the LES-8 underdense and the LES-9 overdense phase data. The striking difference between these pieces of data is the large magnitude of the LES-8 phase fluctuations and the seeming lack of fluctuation activity from the LES-9 data even during strong scintillations. While the LES-8 underdense fluctuations could be ascribed to flight dynamics or oscillator instability, certain facts argue against these explanations. The data from SDS during weak fading establishes a reference for flight dynamics that is several orders in magnitude less than the LES-8 underdense data, thus, for dynamics to be the source of the fluctuations, the flight would have to have been very, and perhaps unreasonably, rough. The LES-8 data from an early portion of the flight in which underdense irregularities were measured show phase fluctuation levels 5 dB less implying that oscillator instabilities probably were not the source of the observed fluctuations. A conservative estimate of the TEC fluctuations from the phase data gives values of $4-8 \times 10^{15}$ electrons per meter squared over 2-4

kilometer structure widths. These enhancements of TEC
are significant and could represent as much as 5-15% of
the background TEC. For comparison, overdense heating
is believed to produce TEC fluctuations of 2-10% of
background (Duncan, 1981, Ref. 3).

Support for the second hypothesis, that underdense
structure is significantly larger in size than structures
produced by overdense heating, comes from the glaring fact
that the AFWAL underdense heating produced little or no
fading whereas the overdense heating produced significant
amounts. The fading produced by overdense heating is
probably more related to the size of the structures instead
of to their intensity. It is conceivable that the phase
fluctuations produced by overdense heating could have sizes
on the order of 100 meters and peak values of approximately
60°. Fluctutations of this nature would produce fading and
phase fluctuations similar to that observed in the data.
Support for the fact that the structures produced by under-
dense heating are large can be found in the fact that when
fading of significant depth is observed in underdense heating
situations as in Basu, et al. (1981, Ref. 7) it is slow and
generally weak. In comparison the fade rate observed in
overdense irregularities is fairly large even at the onset
of irregularity generation.

Backpropagation attempts on the Platteville overdense
data proved unfruitful. This result was expected because
the propagation line-of-sight for this data is within
several degrees of the geomagnetic field. Such geometries
produce signal diffraction patterns which, in general,
should not backpropagate.

4-2   POLAR IRREGULARITIES

Of all the data available for processing, the polar measurements are indicative of the strongest irregularity effects. The r.m.s. phase difference over 1 and 10 seconds and the r.m.s. fading bandwidth are greater than the strong fading from the equatorial data. The polar phase power spectrum is greater than the equatorial phase power spectrum at the very lowest octaves and comparable at the higher frequencies although slightly lower.

Several factors may have contributed to the lack of success of the backpropagation attempts. While the exact geometry is uncertain it may have been close to parallel to the geomagnetic field. The SDS satellite was probably high in its polar orbit. The propagation line-of-sight was, thus, near zenith as is the geomagnetic field.

Another factor may have been structure thickness. Scintillations were observed during the entire four hours of flight test measurements indicating that structure was probably widespread. For a medium to high elevation line-of-sight geometry this fact would tend to imply that structure thickness is a factor in backpropagation processing.

A third factor in back propagation processing is the presence of artifact. This factor certainly affects all the files processed. Phase artifact due to aircraft dynamics and the presence of phase noise spurs such as the harmonic at $2.^{+}$ Hz could contribute to the inability to backpropagate. It should be noted, however, that backpropagation should still be possible in the case where these were the only factors.

75

4-3   EQUATORIAL IRREGULARITIES

The equatorial data is indicative of fairly strong irregularities. The measurements were performed on a flight from Senegal and were made near the geomagnetic equator. The line-of-sight to FLTSAT is at a relatively high angle for the measurement.

Back propagation of the FLTSAT data has shown a consistent local minimum in the value of the scintillation index (normalized r.m.s. power). With a 200 meter per second assumed pattern speed this local minimum occurs near a backpropagation distance of 140 kilometers. No direct phase information is obtainable from the back-propagated field since the minimum scintillation index is still fairly high (.83). From this distance value, however, the true pattern speed may be estimated if it is assumed that the source of the scintillation lies not at 140 km, but instead, in the 300-400 kilometer altitude regime. In this situation the true pattern speed should be scaled to 290-340 meters per second. Assuming a typical 220 meter per second westerly ground speed for the AFWAL 662 aircraft the easterly drift speed of the irregularities is found to be in the range of 70-120 meters per second and in good agreement with other equatorial drift speed measurements.

Given a pattern speed of 100 meters per second it is possible to also derive the r.m.s. angular scatter produced by the medium from the 1.1 Hz r.m.s. fading bandwidth determined in Section 3-3. The result of such a determination yields a value of 9 milliradians of r.m.s. scatter.

Failure of the backpropagation to produce a more significant minimum, i.e., one which would produce a signal phase indicative of TEC fluctuations, can probably be attributed to several factors similar to the case of the

76

polar data processing. The factors which are appropriate
for the equatorial results are oscillator instability,
aircraft dynamics, and structure thickness as discussed
in the previous section, Section 4-2.

4-4   PERU BARIUM STRUCTURE

The Peru barium data has been analyzed in order to
identify the presence of barium structure through the signal
phase. No phase fluctuations that could be clearly identified
as barium related were observed in the processed data.

A phase fluctuation of 1 cycle over an 8 second
interval of the second portion of data is identified in
Section 2-5 as potentially barium related, however it is
also noted that the feature is not correlated with any ampli-
tude fluctuations. As the release occured at a 275 kilometer
altitude and the satellite elevation was close to 35°
during the flight test a 450-500 kilometer slant range to
the barium disturbance can be deduced. Over such a slant
range a Gaussian profile with a 2 kilometer e-folding distance
similar to the one observed would produce at least a 3 dB
amplitude fade which should be observable. Thus, unless the
barium is drifting westerly such that the 8 second interval
represents a pattern distance significantly larger than 2
kilometers, i.e., a westward drift of 100 meters per second
or more, then the phase fluctuation is not barium induced.

Because of the large slant range to the barium cloud
it is possible to argue that amplitude fading is a more
sensitive measure of barium structure presence than is the
phase. In light of the above discussion this argument would
certainly apply to structures smaller than a Gaussian with
2 kilometer e-fold. Amplitude fading results from the first

portion of the data indicate fading of order 1 dB. These effects could be produced by, say, 500 meter structures which to produce the 1 dB fade levels require a hard to detect peak phase shift of 45 degrees.

It is worthwhile to note in retrospect that TEC values comparable to STRESS and PLACES are not expected because of the high release altitude (275 km) and the lesser payload (20 kgm each). Studies by Linson, et al. (1972, Ref. 18) predict peak densities of 1.6×10^6 electrons per cubic centimeter at roughly 1 minute after release. The effects of subsequent ambipolar diffusion may be estimated by assuming a $t^{-1/2}$ diffusion rate over 2000 seconds. A cloud elongation of order forty-to-one is predicted which implies a decrease in density below the 10^5 electron per cc level. At these levels a plasma thickness of 20 kilometers is required to produce a cycle of phase shift on an ideally located propagation path. Thus, it is perhaps expected that no barium induced phase effects are evident in the data.

4-5   AIRCRAFT PLATFORM STABILITY IN STRAIGHT-AND-LEVEL
       FLIGHT

Pearson, Thaller, and Barrett performed a study in 1974 (Ref. 19) of the acceleration levels at various stations onboard the AFWAL 662 aircraft for various modes of flight. Their study presents power spectra of the acceleration fluctuations for straight-and-level flight. This spectrum extends down into the frequency range of interest for phase measurements and has served as a basis for predicting the aircraft platform stability available for such measurements. The phase results of this report

provide a source of comparison for these predictions and a data base for future measurements.

The results of Pearson, et al. demonstrate an acceleration spectral density that is approximately flat and that has an approximate mean power level of 10^{-5} g^2/Hz for straight-and-level flight over the 0.05 Hz to 1.0 Hz frequency interval. From this value, a phase noise value of -48 dB radians squared per Hz at 1 Hz can be derived. An approximate frequency dependence of -40 dB per decade (-12 dB per octave) can also be derived.

The spectral density of the SDS signal phase during the weak fading portion of the polar flight seen in Section 3-2 can be used to estimate upper limits for phase noise arising from flight dynamics over the frequency interval of .003 Hz to roughly .1 Hz. Above .1 Hz weak fading effects should be influencing the data. Table 4-1 shows a comparison of the polar data and the phase noise behavior predicted from acceleration data. The comparison indicates that below .025 Hz the values are in very good agreement differing by at most 4 dB. Above .025 Hz the values differ considerably indicating the likely influence of ionospheric fluctuations in the polar data.

In conclusion, ionospheric fluctuations (or other sources of phase noise) apparently dominate the polar phase spectra over the .05 Hz - 1. Hz frequency range that would directly overlap the acceleration data. However, rough extrapolation of acceleration data to lower frequency does provide results that compare closely with phase noise data in the .003 Hz - .025 Hz frequency interval. A -40 dB/decade spectral dependence with -45 dB radians squared per Hz value at 1 Hz probably provides a realistic estimate of the phase noise arising from aircraft dynamics at frequencies above .003 Hz.

Table 4-1. Phase noise due to aircraft motion.

Frequency	Spectral density (dB rad^2/Hz)	
	Predicted from acceleration measurements of Pearson, Thaller, and Barrett (1974, Ref. 19)	Inferred from polar flight measurements
.00305	53	55
.00610	41	45
.0122	29	30
.0244	16	16
.0488	4	12
.0977	-8	-1
.195	-20	-9

SECTION 5

CONCLUSIONS

A combination of data processing and flight test satellite signal measurements have made possible the display of the phase effects of various ionospheric irregularity environments. Flight test measurements were available from the environments produced by the Platteville heater in both overdense and underdense modes of operation, by the CASTOR equatorial barium release performed by the Max Planck Institute, by polar irregularities and by equatorial irregularities. Section 2 presented the signal amplitude and phase displays resulting from the processing of the data as well as an overview of the processing technique.

The nature of the phase fluctuations measured have been demonstrated in Section 3 both by phase power spectra and by plots of the phase difference standard deviation versus differencing interval. Data was generally available from reference periods during which no signal activity was expected as well as from known periods of activity of interest providing for a clear demonstration of environment effects.

Phase difference histograms are displayed in Section 3-3. These histograms demonstrate the non-Gaussian nature of the phase and phase difference for fading environments. Over short difference intervals the phase difference is distributed in a manner closely approximating the distribution of instantaneous frequency of a band-limited noise process. Thus, the resemblance

between band-limited noise and strong fading is visible
not only in amplitude behavior but also in phase
behavior. The effects of fading on phase shift keyed
systems is discussed in light of the phase distributions
suggested by the histograms. Simple but reasonably
precise expressions for the irreducible error rates are
given in terms of the r.m.s. fading bandwidth. They
imply that a 75 bit per second BPSK system operating
through the polar fading measured could not have reduced
the error rate below 3.2×10^{-3} without the use of coding.
The equatorial environment measured would have experienced
a 1.7×10^{-3} minimum bit error rate. These values
emphasize the importance of the non-Gaussian nature of
the phase.

The phase measurements of the Platteville overdense
and underdense heating environments are probably the first
ever available. They provide startling and potentially
significant results in that they show the TEC fluctuations
produced by underdense heating are significantly greater
in magnitude than those produced by overdense heating.
Underdense heating fluctuations also are fairly large in
scale which explains the absence of corresponding amplitude
fading. Data from overdense heating suggests that the
irregularities may be smaller than the 500 meter scale
size sometimes quoted.

Phase data from the Peru barium release (CASTOR)
did not indicate the presence of barium ion clouds.
It is felt that little or no phase effects should have
been observed because of the high release altitude
(275 km) and fairly low payload (20 kgm). Evidence of
barium cloud presence is probably best indicated by
amplitude fading, some of which was observed during the

latter section of the first portion of data provided
from the flight.

Results from a weak fading portion of the polar
flight test provide a reference file with the least
phase noise in the .003 Hz to .1 Hz spectral range.
The phase noise observed is closely comparable with
predictions based on aircraft acceleration fluctuation
spectral measurements in the .1Hz to 1 Hz spectral
range. The phase noise from aircraft dynamics is, thus,
implied to have a -40 dB/decade dependence over .001
to .1 Hz with a value of about -5 dB radians squared per
Hz at .1 Hz.

During the course of the data processing effort
two algorithms were developed for the improved display
of phase data. An algorithm to compute power spectra
using the sine transform provides more reliable spectra
at lower frequencies. The algorithm takes advantage of
the fact that the sine functions form an orthogonal
basis for the set of linearly detrended phase functions.
An algorithm to draw power law slopes was also developed.
The two algorithms are discussed in the Appendices.

Because of the wide variety of flight test measure-
ments available, a sizable list of recommendations for
future measurements and processing could be given. It
is appropriate to give at least a few.

Because of the potential importance of the under-
dense heating results it is recommended that similar
measurements be made with the use of doppler correction.
While the Platteville heater may be deactivated other
heater experiments are planned in the polar regions in
the winter of 1981. Additional confidence in the results

may also be obtained by processing other intervals of underdense flight measurements and other intervals of no expected activity. In order to facilitate further evaluation of receiver phase noise, processing of satellite phase from intervals when the aircraft is on the ground would also be useful.

To demonstrate irreducible error rate performance predictions measurements of PSK system performance in strong fading would be instructive. Further investigations of phase difference histograms over other fading intervals could also prove to be valuable for demonstrating the likenesses to and differences with band limited noise.

1. A.L. Johnson and R.N. Wright, <u>Platteville flight report</u>, AFWAL Technical Report, 1 September 1980.

2. W.F. Utlaut and E.J. Violette, "A summary of vertical incidence radio observations of ionospheric modification," <u>Radio Science</u>, 9, 895-903, 1974.

3. L.M. Duncan, "Ionospheric modifications by high power radio waves," <u>Proceedings of the 1981 Symposium on the Effects of the Ionosphere on Radiowave Systems</u>, April 1981.

4. C.L. Rufenach, "Radio scintillation of stellar signals during artifical ionospheric modification," <u>J. Geophysical Res.</u>, 78, 5611, 1973.

5. S.A. Bowhill, "Satellite transmission studies of spread-F produced by artificial heating of the ionosphere," <u>Radio Sci.</u>, 9, 975, 1974.

6. S. Basu, S. Basu, A.L. Johnson, J.A. Klobuchar and C.M. Rush, "Preliminary results of scintillation measurements associated with ionospheric heating and possible implications for the solar power satellite," <u>Geophys. Res. Lett.</u>, 7, 1980.

7. S. Basu, S. Basu, S. Ganguly, J.A. Klobuchar and C.M. Rush, "Artificial irregularities generated by ionospheric heating and their effects on transionospheric propatation," <u>Proceedings of the 1981 Symposium on the Effects of the Ionosphere on Radiowave Systems</u>, April 1981.

8. E.J. Fremouw, R.L. Leadabrand, R.C. Livingston, M.D. Cousins, C.L. Rino, B.C. Fair, and R.A. Long, "Early results from the DNA wideband satellite experiment - Complex-signal scintillation," <u>Radio Sci.</u>, 13, 167 1978.

9. S. Basu and J. Aarons, "The morphology of high-latitude VHF scintillation near 70°W," <u>Radio Sci.</u>, 15, 59, 1980.

10. C.L. Rino and S.J. Matthews, "On the morphology of auroral zone radio wave scintillation," <u>J. Geophysical Res.</u>, 85, 4139-4151, 1980.

11. J. Aarons, J.P. Mullen, H.E. Whitney and E.M. MacKenzie, "The dynamics of equatorial irregularity formation, motion and decay," J. Geophys. Res., 85, 139-149, 1980.

12. K.C. Yeh, J.P. Mullen, J.R. Medeires, R.F. da Silva, and R.T. Medeires, "Ionospheric scintillation observations at Natal," Proceedings of 1981 Symposium on Effects of the Ionosphere on Radiowave Systems, April 1981.

13. J.R. Koster, "Phase and amplitude scintillation at the equator," AFGL-TR-78-0289, 31 October 1978.

14. A.L. Johnson and R.L. Swanson, Barium Cloud Test in Peru, AFAL/AAD technical memorandum AFAL-TM-79-15-AAD, July 1979.

15. C.W. Prettie, A.L. Johnson, J.M. Marshall, T.A. Grizinski, and R.E. Swanson, Project STRESS Satellite Communication Test Results, AFAL-TR-77-158, 1977.

16. S.O. Rice, "Mathematical analysis of random noise," from Bell System Technical Journal, vols. 23 and 24, 1944 and 1945; reprinted in Nelson Wax, Noise and Stochastic Processes, New York, Dover, 1954.

17. S.O. Rice, "Statistical properties of a sine wave plus random noise," Bell System Technical Journal, vol 27, pp. 109-157, January 1948.

18. Linson, et al., "Analysis of barium clouds," vol. I, RADC-TR-72-336, AVCO Everett Research Laboratory, Everett, MA, October 1972.

19. J. Pearson, R.E. Thaller, and D.K. Barnett, Test Report on Super High Frequency Communications Terminal Flight Vibration Measurements, Air Force Flight Dynamics Laboratory Report AFFDL/FYS/FYT-74-5, 11 Sept. 1974.

APPENDIX I

DETERMINATION OF THE SINE TRANSFORM AND THE POWER SPECTRAL DENSITY FROM THE TRANSFORM COEFFICIENTS

Suppose a function $g(x)$ is defined over an interval $[0,T]$ and is such that its values are zero at the endpoints of the interval. This function is expandable in terms of the set of sine functions

$$\sin(n\pi x/T) \quad n = 1,2,3,\ldots$$

This set of functions forms an orthogonal basis for the set of all functions like $g(x)$.

The expansion for $g(x)$ is given as:

$$g(x) = \sum_{n=1}^{\infty} a_n \sin(n\pi x/T)$$

where

$$a_n = \frac{2}{T} \int_0^T g(x) \sin(n\pi x/T)\, dx$$

Numerically the coefficients a_n can be evaluated using the FFT algorithm on a set of samples of an extended version of $g(x)$. The extended version of $g(x)$, say $g^*(x)$, is defined by antisymmetrically mirroring $g(x)$ through the value T as follows:

$$g^*(x) = \begin{cases} g(x) & 0 \le x \le T \\ -g(2T-x) & T \le x \le 2T \end{cases}$$

87

The discrete Fourier transform of g^* is a set of imaginary numbers which are seen to be closely related to the sine series coefficients. The discrete expression for the sine coefficients is:

$$a_n = \frac{2}{T} \sum_{m=0}^{N-1} g(m\Delta x) \sin(\pi mn\Delta x/T) \Delta x$$

where $N\Delta x = T$. To relate this expression to the discrete Fourier transform of g^* the sine term is broken into complex exponentials and the sum is reordered:

$$a_n = \frac{2\Delta x}{T} \sum_{m=0}^{N-1} g(m\Delta x) \left\{ \frac{e^{i\pi mn/N} - e^{-i\pi mn/N}}{2i} \right\}$$

$$= \frac{1}{iN} \sum_{m=0}^{N-1} g(m\Delta x) e^{i\pi mn/N} - \frac{1}{iN} \sum_{m=0}^{N-1} g(m\Delta x) e^{-i\pi mn/N}$$

$$= \frac{1}{iN} \sum_{m=0}^{N-1} g(m\Delta x) e^{i\pi mn/N} - \frac{1}{iN} \sum_{k=N+1}^{2N} g(2T - k\Delta x) e^{i\pi nk/N}$$

where k has been set to $2N-m$. The left sum is the contribution to a discrete Fourier transform of $2N$ points of g^* from the interval $0 \le m\Delta x < T$ and the right sum is recognized as the contribution from the interval $T \le m\Delta x \le 2T$ since $g(T) = g(2T) = 0$.

Thus the sine transform coefficients a_n; $n = 1,N$; of $g(x)$ are found to be the negative of the imaginary part

of the first N non-DC coefficients of a 2N-point discrete
Fourier transform divided by N.

To evaluate the power spectral density derived
from the sine transform note that the power in

$$a_n \sin(n\pi x/T)$$

is simply $a_n^2/2$. The terms are spaced uniformly in
frequency with a spacing of $1/2T$. (Note that they are
twice as dense as discrete Fourier transform coefficients
over the interval T.) The power spectral density is thus,

$$\text{p.s.d.} = \frac{a_n^2}{2} \frac{1}{\frac{1}{2T}} = Ta_n^2$$

In terms of the 1st N non-DC imaginary coefficients of a
2N FFT of g^*, f_n, the relation is:

$$\text{p.s.d.} = \frac{T f_n^2}{-N^2} = \frac{\Delta x}{N} f_n^2.$$

APPENDIX II

MAXIMUM LIKELIHOOD ESTIMATE OF POWER LAW SLOPE

Typical slope fits to power spectral data either do not fit the mean power of the spectral components, require significant spectral pre-smoothing or require manual effort. This appendix presents a technique for slope estimation that accounts for the statistics of the power in each of the components of an unsmoothed single DFT spectral estimate and that avoids these disadvantages.

The power component $a(f)$ of a single DFT at spectral frequency f_i is distributed exponentially according to

$$p(a) = \frac{1}{g(f_i)} \exp\left(-a/g(f_i)\right) \quad a > 0$$

where $g(f)$ is the true spectral dependence. The spectral components are generally independent, the only restriction being that $P = \sum_i a(f_i)$, is equal to the total "power" in the data prior to the DFT.

The fit technique is basically to assume a fit dependence $g(f) = A/f^r$ and to maximize the joint density at the occurrence consisting of all the $a(f_i)$ with respect to the spectral slope parameter, r. The factor A is constrained such that the total power in the fit curve and in the data are equal, i.e.,

$$A = P / \sum_i f_i^{-r} ,$$

the sum being over all f which have DFT components. The maximization is, thus, of the product

$$I = \prod_i \frac{f_i^r \sum f_i^{-r}}{P} \exp\left(-a(f_i)\ f^r \sum f_i^{-r}/P\right)$$

90

For convenience the logarithm of this expression is maximized as is typical in maximum likelihood techniques. The logarithm is expressed as:

$$\ln I = r \sum_i \ln f_i - N \ln P + N \ln \sum_i f_i^{-r} - \sum_i (a_i f_i^r \sum f^{-r} / P)$$

where $\sum_i 1 = N$.

Maximization by this technique has been successfully performed numerically. The first two derivatives with respect to r have been analytically formulated and evaluated numerically using an assumed value for r. The index, r, is updated in the direction determined by the first derivative. It is changed according to an amount given by the second derivative only if it is of the proper sign and the change in r determined is less than 1. Otherwise r is changed by 1. Typically convergence to within 10^{-5} is obtained by the end of 8 steps.

For the case of sine transform data the fit routine is fortuitously the same even though the distribution for the spectral coefficients is different.

91